2019

CHARACTERIZATION OF THE IN-PLANE AND CROSS-PLANE THERMAL CONDUCTIVITY OF POLYMER NANOFIBER THIN FILM UTILIZING THE 3-OMEGA METHOD

John P. Carlin
University of Rhode Island, jpcarlin1994@gmail.com

CHARACTERIZATION OF THE IN-PLANE AND CROSS-PLANE THERMAL CONDUCTIVITY OF POLYMER NANOFIBER THIN FILM UTILIZING THE 3-OMEGA METHOD

BY

JOHN P. CARLIN

A THESIS SUBMITTED IN PARTIAL FULFILLMENT OF THE

REQUIREMENTS FOR THE DEGREE OF

MASTER OF SCIENCE

IN

MECHANICAL ENGINEERING

UNIVERSITY OF RHODE ISLAND

2019

MASTER OF SCIENCE THESIS

OF

JOHN P. CARLIN

APPROVED:

Thesis Committee:

Major Professor Carl Rousseau

Yi Zheng

D.M.L. Meyer

Bin Li

Nasser H. Zawia

DEAN OF THE GRADUATE SCHOOL

UNIVERSITY OF RHODE ISLAND

2019

ABSTRACT

The thermal conductivity of Polycaprolactone (PCL) nanofiber thin films produced via an electrospinning method has been studied using the 3ω method. The production process utilized to produce the nanofibers used in this work were selected from a range of tested production processes with preference given to process parameters that produced consistently sized polymer nanofibers, nanofibers devoid of defects, and parameters that increased the general alignment of the resulting PCL nanofiber thin film. The effect of the void portion of a PCL nanofiber thin film is observed with increasing void percentange inversely affecting the effective thermal conductivity of the nanofiber thin film in both the in-planer and cross-planer directions, but increasing the portion of heat energy conducted along the in-planer direction. The data in this work concludes the thermal conductivity of the nanofibers tested is 20% higher in the in-planer direction than in the cross-planer direction, with the highest recorded thermal conductivity being 4.82 $Wm^{-1}K^{-1}$.

ACKNOWLEDGMENTS

I would like to express my very great appreciation to Professor Yi Zheng. During the entire duration of my masters degree, Professor Zheng was always willing and available to discuss the plans and results of my work as well as offer ideas and resources whenever I ran into problems. Prof. Zheng allowed me the final decision on the direction of all experiments and the freedom to organize my results. He has always encouraged deeper learning and was consistently willing to explore new ideas and concepts. Along with Prof. Zheng, I would like to also thank Professor Carl-Ernst Rousseau. Prof. Rousseau kindly stepped in to serve as my major professor when needed in the last month of my degree. He was always available to provide any administrative advice or assistance whenever needed.

I would also like to thank my fellow lab mates for aiding and guiding me throughout; from the inception of this novel design to the final analysis. Alok Ghaneker, Yanpei Tian and Xiaojie Liu all provided good company and fruitful discussion during the entirety of this work. They all made the experience all the more worth it.

Finally, I must express profound gratitude to my friends and family for providing me with unfailing support and continuous encouragement throughout my years of study and through the process of researching and writing this thesis. This accomplishment would not have been possible without them. Thank you.

TABLE OF CONTENTS

Page

Page

LIST OF FIGURES

Figure **Page**

Figure **Page**

LIST OF TABLES

CHAPTER 1

Introduction

When considering the thermal properties of materials while looking for a good candidate material to help in thermal energy management, the first materials one would typically consider would be metals. Having relatively high coefficients of thermal conductivity they are commonly used in heat-sink applications. On the other end of the spectrum however are polymers; with their comparatively low coefficients of thermal conductivity they are regarded as thermal insulators. The reason for their low thermal conductivity is due to a lack of alignment in their polymer chains. This poor alignment results in low phonon energy transfer from lattice vibrations. By manipulating the alignment of these polymer chains into a favorable orientation, the thermal properties of polymers can be significantly enhanced. There exist methods today that do just this with polymers such as the process of electrospinning polymers into nanofibers, which will be discussed further in this work.

Polymers with high coefficients of thermal conductivity are becoming increasing important in today's world. In many fields and practices polymers are becoming increasing favored over other materials such as wood, metal, and ceramics due to its affordability and its ease to work with and shape into many configurations, and the field of thermal management is not ignoring polymers either. As technology pushes the size of components down to the nano-scale, a better understanding of thermal transport of nano-scale devices and individual nanostructures arise [1, 2].

With increasing interest in the applications of polymer nanofibers, the scientific literature generated is accelerating in its ability to find novel uses for this material and understand its intricacies. Current applications for electrospun fibers as

well as their resulting fabrics include filtration [3, 4], drug-delivery systems[5, 6, 7], and biomedical applications, namely in tissue engineering[8, 9].

1.1 Thermal Transport in Nanoscale Structures

Thermal transport occurs in all electrical insulators and semi conductors through the transfer of energy in the form of phonons. These phonons transfer energy through lattice vibrations however themselves have no linear momentum. In bulk materials, the thermal properties of a material are measured statistically, with bulk materials generally being samples with dimensions on scales from millimeters to kilometers [10]. For many materials their thermal properties at the bulk scale are higher than they are at the nanoscale, for some materials such as Silicon, significantly so [11]. There are several exceptions to this generality however, carbon is among the most notable one

1.2 Proposed Method

The process of measuring the thermal conductivity of materials at the micro and nanoscale is a difficult task. Just producing samples at this size is very time, labor, and material intensive. Along with this all quantification tools at this scale are specialized pieces of equipment meant to work at this specific scale. In this section, the different methods of sample production and measurement will be discussed as well as giving justification to the methods selected to complete this work.

1.2.1 Electrospinning

Electrospinning is mainly used to fabricate fibers with diameters ranging from tens of nanometers to a few microns in diameter[12]. Generally electrospinning is done through two different methods. These consist of solution electrospinning as well as melt-electrospinning. In melt-electrospinning, a polymer is heated to its

melting point and charged with a very high voltage to create a nanofiber that collects on a grounded collector[13, 14]. In this version of electrospinning no solvents are needed meaning the solvent does not contaminate the final nanofiber product. Melt-electrospinning can fabricate nanofibers at room temperature from polymers with low melting temperatures, such as polyethylene (PE), polypropylene (PP) and polyethylene terephthalate (PET)[15].

The other form of electrospinning is solution based electrospinning. This process is affected by more parameters than its melt-electrospinning variation, of which can be seen in Table 1, but allows for more control over the resulting fibers and for a wider range of workable polymers and enhancing materials. In this work however solution electrospinning is the method that was used to produce any nanofiber mentioned from here onward.

Table 1. Parameters That Affect Electrospinning from Polymer Solutions

Solution Parameters	Process Parameters	Ambient parameters
Molecular weight of the polymer Concentration of solution Viscosity Surface Tension Solvent properties	Applied Voltage Tip to Target Distance Type of collector Flowrate of polymer solution	Temperature Humidity

In the solution electrospinning method, a polymer solution is pumped at a constant rate through a positively charged electrode, which then travels through a high voltage electric field to a grounded collector plate. This induced electric field causes the electrode to positively charge the polymer solution at its tip. The droplet of solution that collects at the tip of the electrode is thus deformed as it tries to repel the homogeneous positive ions it has collected. When the applied voltage reaches a critical value, the deformed droplet finally ejects a charged jet from the tip of the cone that accelerats towards the grounded collector. As this jet

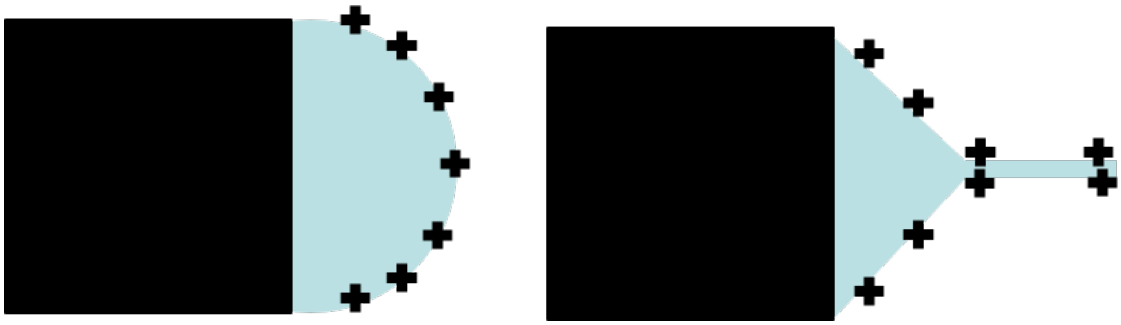

Figure 1. The formation of a Taylor Cone on a positively charged electrode

accelerates towards the collector, the solution evaporates leaving only the polymer that was dissolved into it, being collected in continuous fibers.

The ejection of a charged jet from the deformed droplet has been well studied and has been determined to be the result of the formation of a phenomena known as a Taylor Cone. This theory is first stated by Taylor in 1964 [16]. As the solution continues to collect and simultaneously repel itself at the tip of the electrode, the surface tension of the solution holds it together until the surface forces are overcome by the attractive force of the oppositely charged grounding electrode. As this voltage differential increases, the droplet at the electrode will continue to elongate to a conical shape, a Taylor Cone. Taylor characterized the relationship between the electric field E, the solutions surface tension σ and the curvature of the Taylor Cone, r. In this relation ϵ_0 is the permittivity of free space, and α being the half angle of the cone.

$$\frac{1}{2}\epsilon_0 E^2 = \frac{\sigma}{r tan(\alpha)} \tag{1}$$

Due to imperfections that cause concentrations of positively charged ions along the axis of the elongated polymer fiber that is ejected from the Taylor Cone, the fiber will experience a whipping process. This process further elongates the fiber and increases the rate of evaporation of the solvent. The formation of a Taylor Cone as the voltage differential reaches its critical value is depicted in Fig 1.

1.2.2 SEM Use

A scanning electron microscope (SEM) is a type of microscope that uses a focused beam of electrons to produce an image at a far greater magnification and resolution than traditional optical microscopes. Samples imaged through SEM are typically electrically conductive, as without this property negative charges quickly accumulate within a sample and create a sort of over-exposed image when observing the sample. Polymers are typically among such materials that have low electrical conductivity and produce poor resolution images in SEM machines. The high power electron beam can quickly damage the sample leaving visible scars on the sample and also rapidly accumulate negative charges from the electron beams[17]. There are however methods to get around this on SEM machines to produce high quality images of the orientation and morphology of electrospun polymer nanofibers. Through the use of a low-voltage scanning mode these nanofibers can be imaged[18]. The SEM used in this work is a Field Emission SEM purchased from Zeiss microscopy, Fig. 2.

In order to obtain these sharp images at the necessary size scale and resolution an unusually low electron beam power was used for the sample. Typically when using SEM for nano and micron scale microscopy a 3 keV electron beam is used. As per the concerns pointed out in this section however, this would cause far too much of a negative charge to build in the sample and would quickly damage the sample used in this work. An electron beam of power 1.1keV was used instead. with proper adjustments to the aperture and signal of the SEM the polymer nanofibers were able to be successfully imaged. There is still some minor scarring on the samples as a result of the electron beam, however SEM shows to be an effective method to evaluating the morphology of individual nanofibers and determining the alignment of nanofiber supported thin films. See Fig. 3 to reference the result of

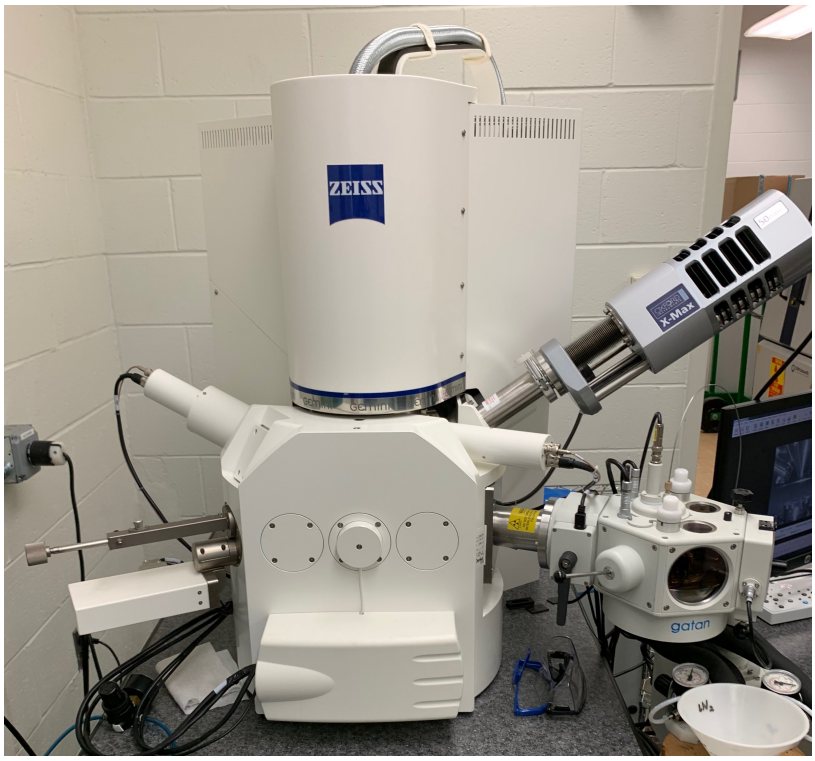

Figure 2. Scanning electron microscope from Zeiss Microscopy

the SEM validity test on examining polymer nanofibers.

Various other surface characterization techniques are available to use to define the structures of the nanofiber thin films. Atomic Force Microscopy (AFM) is an option available for measuring surface roughness of various materials, including thin films. AFM is able to determine the arrangement of individual polymer chains and molecules in a sample with high accuracy without the use of any destructive techniques to the individual sample [19, 20]. Despite the AFM's high accuracy in measuring surface topologies, the SEM will be used for the majority of the nanofiber thin film imaging in this work due to the images produced by SEM being more workable and being able to measure multiple characteristics from a single image.

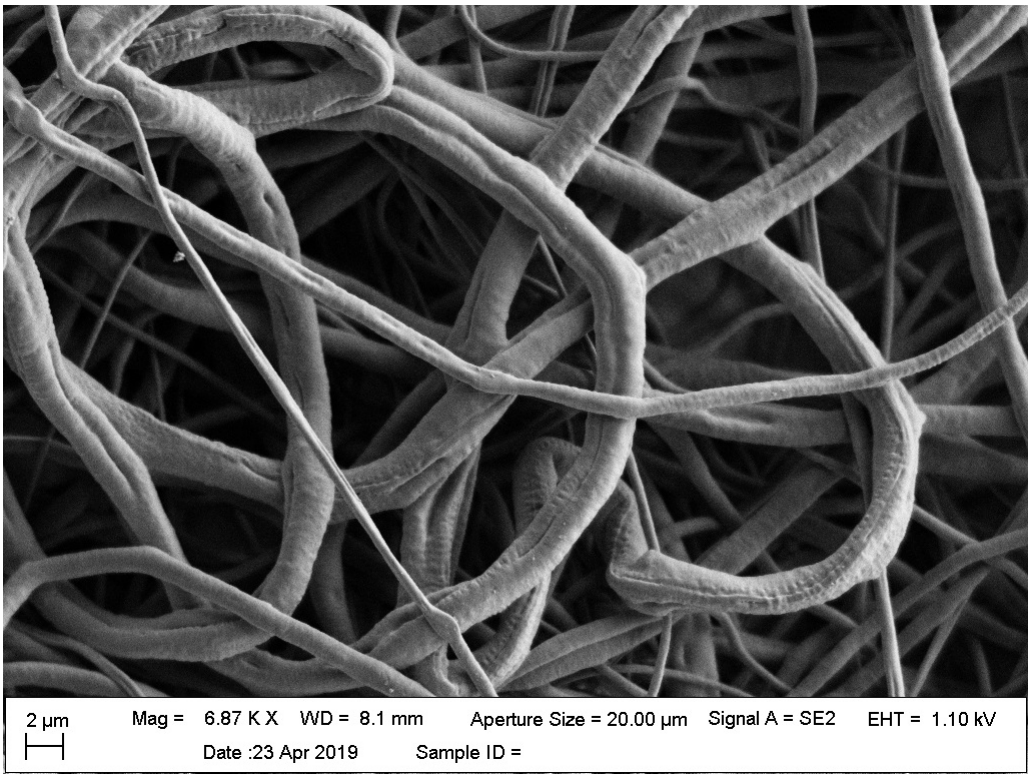

Figure 3. SEM Imaging of polymer nanofibers at 6870x magnification

1.2.3 3ω Method

Measuring the thermal properties of micro and nanoscale materials is no simple process. Along with the challanges associated simply with the small geometry of the samples, when trying to measure the thermal conductivity of small solids, the heat transfer can very easily be dominated by heat transfer from convective sources as well as heat transfer through radiation.

A solution to this issue has been shown in the form of the 3ω method. This method is first described by David G. Cahill in 1990 [21]. This work uses a single wire like heating element powered by an alternating current. This heating element works as both the sample heater as well as a sample thermometer by measuring the frequency dependence of the sample's temperature oscillations. In this method the temperature of the sample is measured by the third harmonic of the voltage

across the metal line. This occurs due to joule heating occuring at 2ω with an input current at angular frequency ω. As the temperature of the sample increases the resistance of the metal line will also increase making the resistance of the metal line also a function of ω, oscillating at 2ω. When multiplying the original input current oscillation by the resistance oscillation, as per Ohm's law (Eq.2) the resulting voltage oscilation will be at frequency 3ω.

$$V(\omega) = I(\omega) * Z(\omega) \tag{2}$$

The amplitude of the measured voltages at frequency 3ω can then be related back to the heat capacity as well as the thermal conductivity of the sample it is measuring. Along with the 3ω's novel method of measuring the thermal conductivity of thin films it also has several advantages over conventional thermal property measurement techniques. The 3ω method is capable of measuring the thermal conductivity of a sample at a very large range of temperatures, as extreme as 30 K to 750 K has already been proven viable [21]. In addition to operating at these temperature extremes the method also determines all of these thermal properties in as short a time as periods of the frequency of the input current into the 3ω metal line, which is no more than a few seconds. This totally bypasses the usual need of conventional thermal measurement techniques of keeping a sample at a controlled temperature for a long enough time to reach steady state, which can take hours to perform full tests. The 3ω heater design geometry used in this work is shown in Fig 4.

The exact 3ω method used has several key modifications made to it when compared to Cahill's apparatus as described in his original work on the method. The details of these modifications will be explained later, but what they accomplish is quite significant. The first outcome of these modifications is the introduction of a Wheatstone bridge in the 3ω test platform. Through the use of this simple circuit

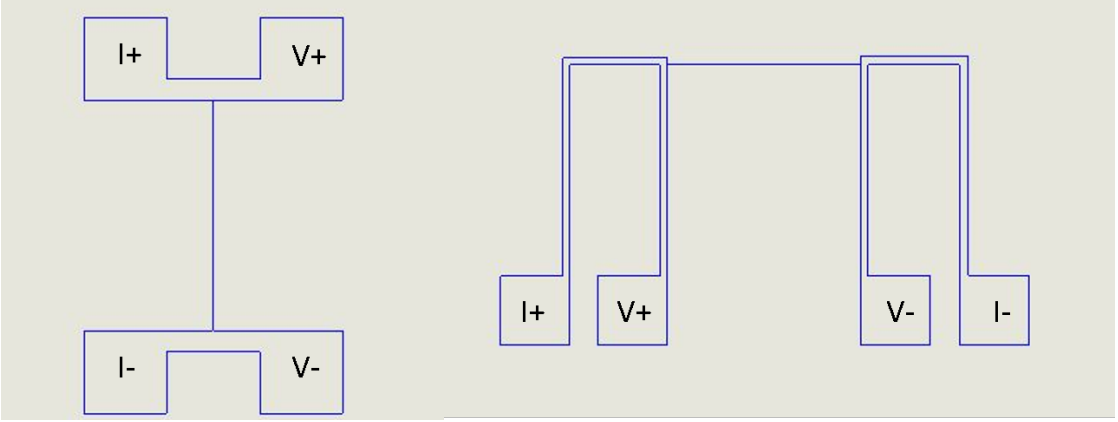

Figure 4. Geometry and pad input/outputs of the 3ω design used in this work

calibration of the experimental apparatus can be conducted much more swiftly and accurately [22]. The following modification is to deposit the 3ω test platform onto one substrate, and the test sample onto another. This method is necessary for the type of testing conducted in this work but has the added benefit of not requiring the testing to be conducted in a vacuum chamber due to reduced heat transfer through convection [23]. While these modifications have individual benefits, combined they also result in significant cost savings. Tests conducted without the ability to make these modifications frequently need to purchase custom equipment and have their 3ω test platform fabricated on printed circuit-boards. A full custom 3ω platform can cost $20,000 to produce [24], a cost that can be virtually completely ignored in this work.

1.2.4 Other Considered Thermal Conductivity Measurement Methods

Alongside the 3ω method of measuring the thermal conductivity of electrospun nanofibers. Among the other methods considered is the T-type method of measuring thermal conductivity. This method has successfully measured the thermal conductivity of fibers of many materials that are too thin to measure using conventional methods [25, 26, 27]. The T-type method is similar to the 3ω method

in that both use a metallic calibration material with a known thermal conductivity to act as both a heater and a thermometer of the sample it is measuring. Unlike the 3ω method however the thermal conductivity of the material is measured using a direct current instead of an alternating current. The T-type thermal conductivity measurement method relies on measuring the one-dimensional steady-state heat conduction through a material. By measuring the thermal expansion of the sample material as well as the temperature at all three points on the T-type measurement platform the thermal conductivity of the sample can be determined. While this method is promising in measuring the thermal properties of materials which are too small to be measured by conventional methods, it specializes in measuring individual fibers, something that is not looking to be measured in this work. Along with this this method must take into account heat loss from radiation, for these reasons the 3ω method for measuring the thermal conductivity of a sample was chosen.

Another considered method for thermal measurements in this work were the Time Domain Thermoreflectance Method (TDTR) as well as the Frequency Domain Thermoreflectance Method (FDTR). Both of these methods are non contact techniques that use optical lasers to characterize the thermal properties of a sample. This laser focuses on a sample and provides energy to the sample which heats it and then measures the change in reflectively of the sample as it heats. In able to properly utilize this method however, a laser that operates at an incredibly short time constant must be used, this ensures that only the surface of the sample is heated to prevent any thermal contribution from the substrate the thin film is prepared on (picosecond resolution)[1].

Similar to most Scanning Electron Microscope (SEM) imaging, the samples measured in this method require a very thin layer (about 80 nm) coating of a high

conductivity material. This method however requires this coating to use it as a reflective surface to measure the thermal properties, and as the polymer nanofibers used in this work are quite dull this coating is required. This method is quite intensive to set up but accurately characterizes the thermal conductivity of thin films [28, 29]. This method has successfully characterized the thermal properties of bulk materials [30], liquid compounds [31], and conductive thin films without an additional metallic thin layer [32]. While this is a very powerful tool in measuring the cross-plane thermal conductivity of materials, no literature on it successfully measuring in-plane thermal conductivity's were found.

List of References

[1] D. G. Cahill, W. K. Ford, K. E. Goodson, G. D. Mahan, A. Majumdar, H. J. Maris, R. Merlin, and S. R. Phillpot, "Nanoscale thermal transport," *Journal of Applied Physics*, vol. 93, no. 2, pp. 793–818, 2003.

[2] D. G. Cahill, P. V. Braun, G. Chen, D. R. Clarke, S. Fan, K. E. Goodson, P. Keblinski, W. P. King, G. D. Mahan, A. Majumdar, *et al.*, "Nanoscale thermal transport. ii. 2003–2012," *Applied Physics Reviews*, vol. 1, no. 1, p. 011305, 2014.

[3] A. Wilson, "Autofluorescent imaging and target ablation," U.S. Patent 8 160 680, Apr. 17, 2012.

[4] P. P. Tsai, H. Schreuder-Gibson, and P. Gibson, "Different electrostatic methods for making electret filters," *Journal of Electrostatics*, vol. 54, no. 3-4, pp. 333–341, 2002.

[5] Y. K. Luu, K. Kim, B. S. Hsiao, B. Chu, and M. Hadjiargyrou, "Development of a nanostructured DNA delivery scaffold via electrospinning of PLGA and PLA-PEG block copolymers," *Journal of Controlled Release*, vol. 89, no. 2, pp. 341–353, 2003.

[6] J. Zeng, X. Xu, X. Chen, Q. Liang, X. Bian, L. Yang, and X. Jing, "Biodegradable electrospun fibers for drug delivery," *Journal of Controlled Release*, vol. 92, no. 3, pp. 227–231, 2003.

[7] G. Verreck, I. Chun, J. Rosenblatt, J. Peeters, A. Van Dijck, J. Mensch, M. Noppe, and M. E. Brewster, "Incorporation of drugs in an amorphous state into electrospun nanofibers composed of a water-insoluble, nonbiodegradable polymer," *Journal of Controlled Release*, vol. 92, no. 3, pp. 349–360, 2003.

[8] N. Bhattarai, D. Edmondson, O. Veiseh, F. A. Matsen, and M. Zhang, "Electrospun chitosan-based nanofibers and their cellular compatibility," *Biomaterials*, vol. 26, no. 31, pp. 6176–6184, 2005.

[9] C. Y. Xu, R. Inai, M. Kotaki, and S. Ramakrishna, "Aligned biodegradable nanofibrous structure: A potential scaffold for blood vessel engineering," *Biomaterials*, vol. 25, no. 5, pp. 877–886, 2004.

[10] E. Roduner, "Size matters: why nanomaterials are different," *Chem. Soc. Rev.*, vol. 35, pp. 583–592, 2006.

[11] L. M. Jiji, "Microscale conduction," *Heat Conduction: Third Edition*, vol. 35, pp. 347–401, 2009.

[12] D. Li and Y. Xia, "Electrospinning of nanofibers: Reinventing the wheel?" *Advanced Materials*, vol. 16, no. 14, pp. 1151–1170, 2004.

[13] P. D. Dalton, D. Grafahrend, K. Klinkhammer, D. Klee, and M. Möller, "Electrospinning of polymer melts: Phenomenological observations," *Polymer*, vol. 48, no. 23, pp. 6823–6833, 2007.

[14] P. D. Dalton, J. L. Calvet, A. Mourran, D. Klee, and M. Möller, "Melt electrospinning of poly-(ethylene glycol-block-ϵ-caprolactone)," *Biotechnology Journal*, vol. 1, no. 9, pp. 998–1006, 2006.

[15] R. Nayak, I. L. Kyratzis, Y. B. Truong, R. Padhye, L. Arnold, G. Peeters, L. Nichols, and M. O'Shea, "Fabrication and characterisation of nanofibres by meltblowing and melt electrospinning," *Advanced Materials*, vol. 472, pp. 1294–1299, 3 2012.

[16] G. I. Taylor, "Disintegration of water drops in an electric field," *Proceedings of the Royal Society of London. Series A. Mathematical and Physical Sciences*, vol. 280, no. 1382, pp. 383–397, 1964.

[17] B. Cheney, "Introduction to scanning electron microscopy," *Materials Engineering department San Jose State University*, 2007.

[18] C. Gaillard, P. A. Stadelmann, C. J. G. Plummer, and G. Fuchs, "Practical method for high-resolution imaging of polymers by low-voltage scanning electron microscopy," *Scanning*, vol. 26, no. 3, pp. 122–130, 2004.

[19] R. Jagtap and A. Ambre, "Overview literature on atomic force microscopy (afm): Basics and its important applications for polymer characterization," 2006.

[20] P. Eaton and P. West, *Atomic force microscopy*. Oxford University Press, 2010.

[21] D. G. Cahill, "Thermal conductivity measurement from 30 to 750 k: the 3 method," *Review of Scientific Instruments*, vol. 61, no. 2, pp. 802–808, 1990.

[22] T. Yamane, N. Nagai, S.-i. Katayama, and M. Todoki, "Measurement of thermal conductivity of silicon dioxide thin films using a 3-omega method," *Journal of Applied Physics*, vol. 91, no. 12, pp. 9772–9776, 2002.

[23] X. J. Hu, A. A. Padilla, J. Xu, T. S. Fisher, and K. E. Goodson, "3-Omega Measurements of Vertically Oriented Carbon Nanotubes on Silicon," *Journal of Heat Transfer*, vol. 128, no. 11, p. 1109, 2006. [Online]. Available: http://heattransfer.asmedigitalcollection.asme.org/article.aspx?articleid=1448515

[24] N. AL-KHUDARY, "Material thermal conductivity mesurement by the 3-omega method application to polymer characterization using inkjet printing technology," *These*, p. 264, 2014.

[25] X. Zhang, S. Fujiwara, and M. Fujii, "Measurements of thermal conductivity and electrical conductivity of a single carbon fiber," *International Journal of Thermophysics*, vol. 21, no. 4, pp. 965–980, 2000.

[26] C. Lu, S. Wai, H. Du, J. Li, L. Gan, X. Zhang, X. Chu, Y. Yao, B. Li, and F. Kang, "Thermal conductivity of electrospinning chain-aligned polyethylene oxide (PEO)," *Polymer*, vol. 115, pp. 52–59, 2017.

[27] J. L. Wang, M. Gu, X. Zhang, and Y. Song, "Thermal conductivity measurement of an individual fibre using a T type probe method," *Journal of Physics D: Applied Physics*, vol. 42, no. 10, 2009.

[28] H. K. Lyeo, D. G. Cahill, B. S. Lee, J. R. Abelson, M. H. Kwon, K. B. Kim, S. G. Bishop, and B. K. Cheong, "Thermal conductivity of phase-change material Ge 2 Sb 2 Te 5," *Applied Physics Letters*, vol. 89, no. 15, pp. 87–90, 2006.

[29] Y. K. Koh and D. G. Cahill, "Frequency dependence of the thermal conductivity of semiconductor alloys," *Physical Review B - Condensed Matter and Materials Physics*, vol. 76, no. 7, pp. 1–5, 2007.

[30] R. M. Costescu, M. A. Wall, and D. G. Cahill, "Thermal conductance of epitaxial interfaces," *Physical Review B - Condensed Matter and Materials Physics*, vol. 67, no. 5, pp. 1–5, 2003.

[31] A. J. Schmidt, X. Chen, and G. Chen, "Pulse accumulation, radial heat conduction, and anisotropic thermal conductivity in pump-probe transient thermoreflectance," *Review of Scientific Instruments*, vol. 79, no. 11, 2008.

[32] J. P. Feser, J. Liu, and D. G. Cahill, "Pump-probe measurements of the thermal conductivity tensor for materials lacking in-plane symmetry," *Review of Scientific Instruments*, vol. 85, no. 10, 2014.

CHAPTER 2

Experimental Apparatus

This chapter will review the electrospinning apparatus used for fiber fabrication, as well as the 3ω method that is used to characterize the thermal conductivity of the polymer nanofiber supported thin films.

2.1 Nanofiber creation

The nanofibers used in this work are created through an electrospinning process. In this process a polymer is dissolved into a natural solvent at a certain weight percentage, defined by the following equation.

$$\frac{w}{v}\% = \frac{mass\ of\ the\ solute\ w_x}{volume\ of\ the\ solution}\ x\ 100 \tag{3}$$

This specific solution used in this work is a 12 wt% of Polycaprolactone (PCL) supplied by Aldrick Chemistry dissolved in Acetone ($\geq$ 99.9%) purchased from Sigma Aldrich. This solution was prepared by adding 24 g of PCL to 200 mL of Acetone on a hot plate at 40 °C which is being mechanically agitated by a magnetic stir bar at 600 RPM. After mixing for 3 hours the PCL is fully dissolved into the PCL/Acetone solution and it is stored in an oven kept constantly at 60 °C for storage.

When spinning the nanofibers, the solution is loaded into a 30 mL syringe which is further placed into a 2 channel syringe pump. Nanofibers spun in this work were spun using the syringe pump depicted in Fig. 5 with varying syringe flow rates ranging from 5 to 12 mL/h. The varying flow rates in this work are used to generate nanofibers with varying cross sectional areas, with slower flow rates producing nanofibers with smaller cross sections than the nanofibers produced at higher flow rates. The flow rates must remain high enough however to maintain a

Taylor Cone at the tip of the spinnerets. While not used particularly in this work this syringe pump has the capability of pumping two solutions simulataneously. This is useful when producing nanofibers with a core-shell geometry which will be expanded upon in the future work section.

Using the prepared solution in a syringe placed into a syringe pump, an appropriate flow rate for the solution is determined. This is done by applying a flow rate and observing the spinneret electrode for the solution. The solution should form a drop at the tip of the spinneret electrode, when this drop falls, an appropriate flow rate will result in a drop reforming at the tip of the spinneret immediately. In this work, a flow rate of 7ml/hr was determined as the minimum appropriate flow rate. After determining the appropriate flow rate of the solution, the critical voltage differential is determined for the proper formation of a Taylor Cone on the spinneret. Taylor expressed a relation between solution properties and spinneret properties for determining the critical voltage[1]. This is expressed as:

$$V_c^2 = 4\frac{H^2}{L^2}(ln\frac{2L}{R} - 1.5)(0.117\pi R\sigma) \tag{4}$$

Here H is used to describe the Tip to Target distance, L is the length of the needle, R is the radius of the needle, and σ is the surface tension of the solution. This relation can be used to determine the critical voltage empirically. However the electrospinning apparatus used in this work allows for the critical voltage to be determined experimentally by simply increasing the voltage differential until a Taylor Cone forms at the tip of the spinneret and maintains a continuous jet between the spinneret electrode and the collector. The determined critical voltage in this work was found to be +20kV using a tip to target distance of 15 cm.

The syringe pump pumps the solution through a hose and into the electrospinning apparatus. The electrospinning apparatus used in this work is a TL-Pro-BM Robotic Electrospinning setup purchased from Tong Li Tech Electrospinning. This

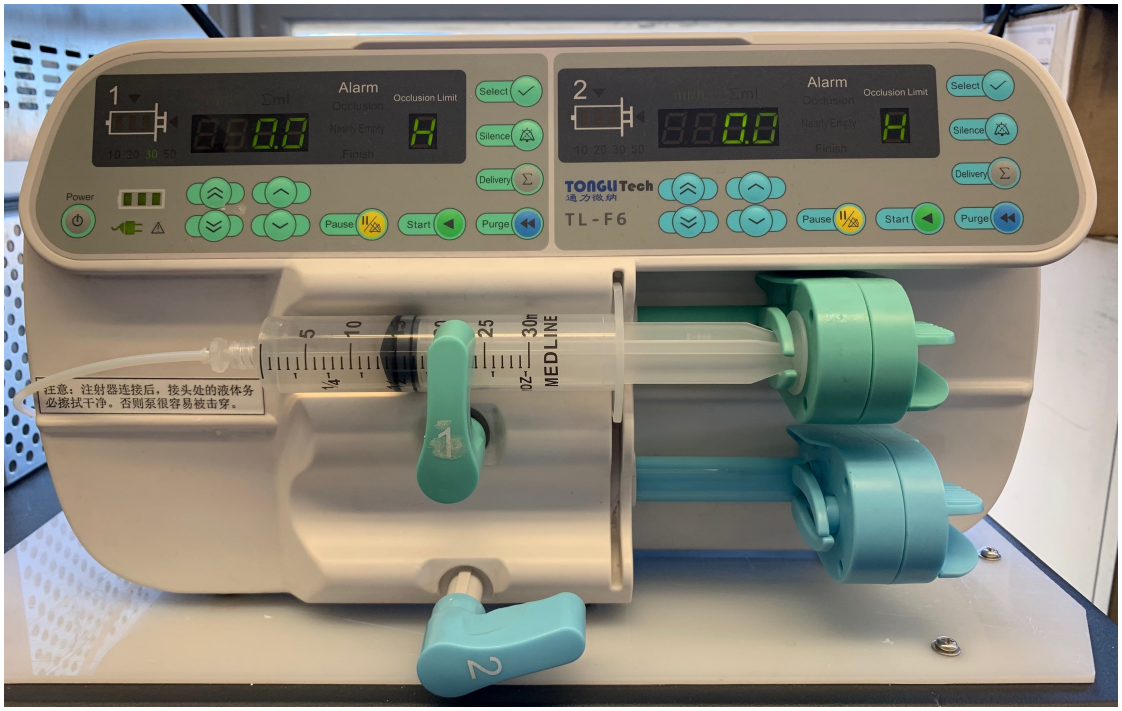

Figure 5. Dual Channel Syringe Pump

Table 2. Settings and materials utilized in producing highly aligned nanofiber supported thin film

Spinneret Voltage	+18k V
Collector Voltage	-2k V
Drum Rotation	250 RPM
Drum Acceleration	50 RPM/s
Tip to Target Distance	15 cm
Scan Distance	175 mm
Needle Size	20 AWG

Figure 6. Electrospinning apparatus supplied by Tong Li Tech

machine depicted in Fig. 6 is the main setup used in this work. This machine is configured to the settings in Table 2 in order to produce highly aligned polymer nanofibers.

The electrospinning spinneretts used in this work are 20 AWG 1/2" industrial dispensing tips purchased from CML supply. These needles are arranged in a 1 x 5 array orientation with all of the needles receiving the polymer solution in parallel. These needles are all brought to a +18k voltage differential simultaneously and sweep across the collector drum to apply an even coat of electrospun nanofibers to the collector drum. The arrangement of the electrospinning spinnerets can be seen in Fig. 7.

To collect the polymer nanofibers, the TL-Pro-BM comes with a modular base collector that allows for the collector to be swapped out to a number of different

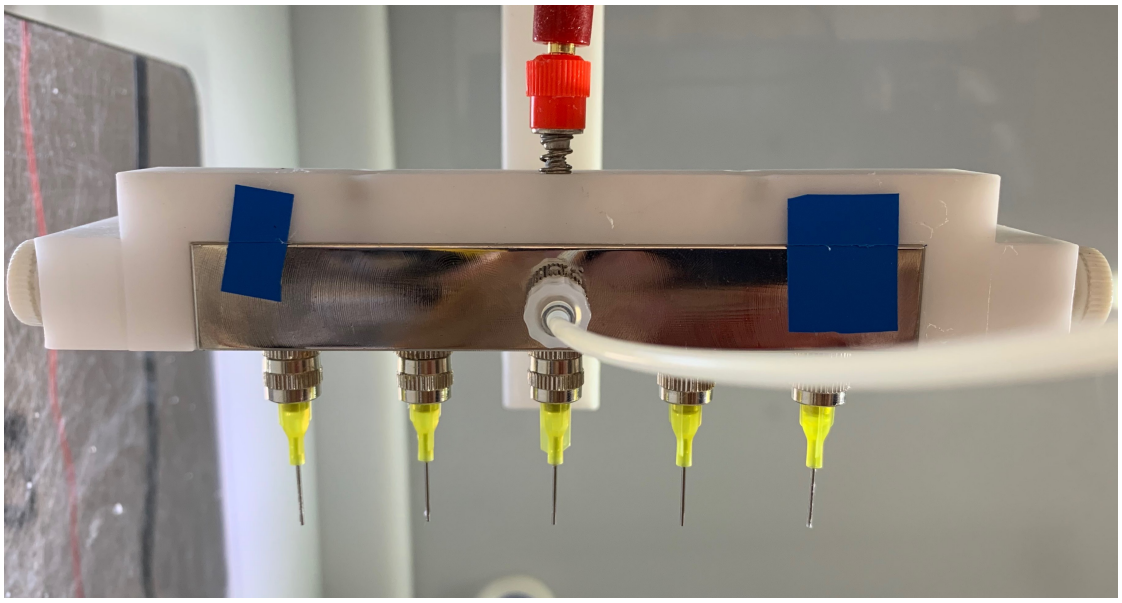

Figure 7. Spinneret orientation of Electrospinning device

collectors that serve different purposes. The collector used to produce well aligned polymer nanofibers was a rotating drum collector. This collector was set to rotate at 250 RPM in order to collect the fibers in a fashion that orientates these fibers parallel to the instantaneous velocity of the cylinder's surface. This cylinder is 30 cm long and has a diameter of 10 cm. In order to collect the nanofibers for measurement, the cylinder is coated in a layer of tin foil and has 3 microscope slides appended to it. The microscope slides, Fig. 8, are arranged in groups of three in order to collect multiple samples from the same run of tests. One of the slides has the nanofibers harvested from it in order to examine the alignment of the nanofibers in the scanning electron microscope (SEM), another is used in the testing of its effective thermal conductivity, and the third is left untouched as a reference sample.

2.1.1 Temperature and Humidity Contribution

Reproducing nanofibers of comparable quality is also a difficult task to complete. Beyond the simple controllable variables of solution parameters as well as

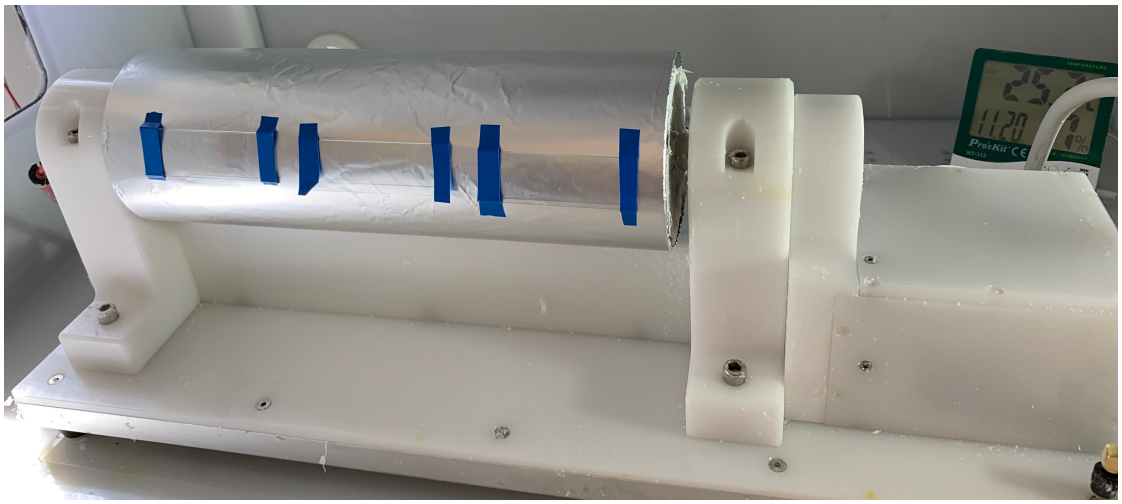

Figure 8. TL-Pro-BM rotating drum collector with appended microscope slides

the electrospinning settings, the environment in which nanofibers are electrospun in has a major role in the morphology of the fibers. Determining and predicting the effect of specific environmental conditions on a nanofiber solution is a major topic of study in the field of electrospinning as well as a large obstacle to the success of electrospinning in industry[2]. While the ambient conditions that the nanofibers were produced in in this work were not controlled, they were considered. Studies have been conducted to determine the effect of ambient conditions on the morphology of electrospun nanofibers taking into account ambient temperature and relative humidity.

The common finding when observing the effects of ambient temperature and relative humidity on the morphology of a nanofiber, is the formation of crater-like pores on the surface of the polymer nanofibers with increasing relative humidity. Increasing the ambient temperature that the polymer nanofibers are produced in has a dampening effect on the formation of these pores, requiring an increase in relative humidity to produce the same porous morphology on a sample produced at a higher ambient temperature as it does one produced at a lower ambient temperature. There are two common explanations that describe the formation of these

pores [2].

1. The pores are the result of water droplets that have formed on the surface of the polymer solution jet, with increasing frequency as the humidity increases as a result of a more probable chance of reaching the dew point of water.

2. The presence of water in the ambient air resulting in a phase separation in the polymer solution jet into polymer-rich and polymer-poor sections. This phase-change likely caused by the water-rich ambient air causing a temperature drop at specific points along the polymer solution jet.

2.1.2 Nanofiber Dimensions

During the creation of nanofibers, much of the determining factors on the diameter of resulting nanofiber occur in the gap between the spinneret and the collector[3]. As the nanofiber solution exits the spinneret, the jet will have a small segment were it travels in a straight line. This straight segment is immediately followed by a boil of increasing diameter caused by bending instabilities. Bending instabilities in the electrospinning process are described in Taylor's original work on the topic and are characterized for small perturbations [4], and have also been expressed as mutual Coulomb interactions caused by the uniformly distributed electrical charge in the polymer jet[5]. After several turns of this coil, the process repeats as a new bending coil forms in the jet causing a smaller coil to form about the path of the original coil. This process repeats again and will further continue until the electrically caused elongation of the polymer solution stops, which normally coincides with the solidification of the polymer nanofiber[6]. In Fig. 9 the first order bending instabilities result in the orange coil, with the second and third bending instabilities resulting in the green and blue coils respectively.

The coils that form from the bending instabilities in the fiber are only one

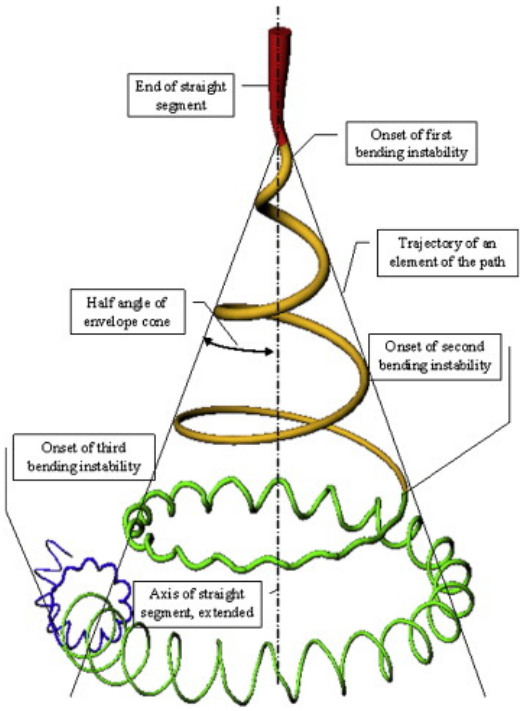

Figure 9. Bending instabilities in the polymer solution jet during a typical electrospinning process [6]

example of the instabilities that occur in the formation of the polymer nanofibers. In addition to these instabilities, branching and the formation of beads in the nanofibers also occurs in specific conditions. The first of these instabilities, branching, is the result of excess of charge by increasing the potential difference in the nanofiber solution [6]. These branches form outward from the center of the nanofiber solution and are dominated by the electric field that results from the positively charged nanofiber solution jet, but also effected by the voltage differential between the spinneret electrode and the collector. The resultant of these forces develops a branch that grows radially outward from the center of the nanofiber solution jet with a small downward component due to the potential difference between the spinneret electrode and the collector. The formation of these branches can be relatively controlled through a single process variable in the formation of these nanofibers [7]. The distance between the formed branches has been shown

to decrease as the potential difference between the spinneret and the collector is increased. This leads to the conclusion that decreasing the potential difference between the spinneret and the collector to a point that still maintains a Taylor Cone results in far fewer, or possible elimination of branches from the polymer solution jet.

The second form of instability in nanofiber production is the formation of beads along the fiber. The formation of thin nanofibers with periodic relatively large beads is the result of a lower surface energy compared to maintaining a fiber of a consistent unbeaded cylindrical form [6, 8]. The best practice to avoid this outcome is to maintain a high enough voltage differential between the spinneret electrode and the collector. Previous work into the phenomena [8], showed that by surrounding the air around the polymer solution jet with a neutralizing ion stream through a corona discharge leads to a significant increase in beaded fibers. The conclusions drawn from this work show that by maintaining a sufficiently high potential difference between the spinneret and the collector the polymer solution is actively being stretched and forced into a consistent diameter until the point that the solution is fully evaporated and the nanofiber solidifies. Both the formation of beads and branches are in this work non-favorable instabilities in the formation of nanofibers and require opposite calibration of the potential difference between the spinneret and the collector to be avoided. Due to this the formation of one branching is favored over the formation of beading. A higher voltage potential is used as the formation of branching tends to be limited to the early regime of the polymer solution jet, the straight segment and the first bending instability.

2.1.3 Nanofiber Alignment

The orientation of a nanofiber sheet is largely determined by the method in which it is collected. The most common method of collecting nanofibers in such

a way that they are oriented largely parallel to each other, is to collect them on a rotating collector. By grounding a rotating drum, the generally randomly oriented nanofibers will begin to orient themselves tangentially to the axis of rotation on the drum collector. The rotational velocity needed to produce aligned nanofibers is generally referred to as the critical uptake speed, and it is generally normalized into a tangential velocity in m/s rather than rotations per minute (RPM) to account for electrospinning apparatus of varying drum diameters. Various works have the critical uptake speed for electrospun nanofibers to be in the range of several meters per second [6]. However electrospun PCL nanofibers specifically have been found to have a critical uptake speed of about 1.7 m/s [2]. Other works have been published showing SEM images of aligned fibers collected at incredibly high uptake velocities, almost 10 times the previous value at 15.7 m/s [9]. When the uptake velocity reaches much higher than 2.5 m/s the air around the collector becomes more turbulent, negatively impacting the alignment of the nanofibers as they reach the collector. This is reversed however at even higher uptake velocities as the collector pulls the fiber onto itself at a much higher rate, stretching it in the process.

2.2 3ω test platform fabrication

The 3ω test platform for this work is produced through a photo lithography and sputtering dual process. In total eight 3ω metal lines of various geometries and sizes were produced, each meant to test the cross plane thermal conductivity, the trans-axial cross plane thermal conductivity or the in-plane thermal conductivity of the nanofiber thin film.

The production of the metal lines started with a simple calculation to determine the necessary line thicknesses from estimates of the expected thermal resistance of the thin film and the thickness of the thin film produced. To determine the necessary sizes of the 3ω metal line, the following equation was used, where b

is one half of the metal line width and d_f is the thickness of the film it is measuring. The resultant of this equation is a unitless numbers that describes if the joule heating from this process will be in-planer or cross planer. heating[10, 11]. This term can be thought of as the heating thickness regime, and it defines if the joule heater is considered a thick or thin heater.

$$\omega_t = (\frac{b}{d_f})(\frac{\lambda_z}{\lambda_x})^{\frac{1}{2}} \tag{5}$$

When this term is large, above 0.5, with a $\frac{b}{d_f}$ of 2.5 or greater[12], the heating will be entirely dominated by cross planer heating. The opposite extreme is also true however when ω_t is small, under 0.1, where the joule heating will result entirely in in-planer heating. [10, 11]. Due to all of the nanofibers being oriented parallel to each other, the sample may also be turned 90° to determine the trans-axial thermal conductivity.

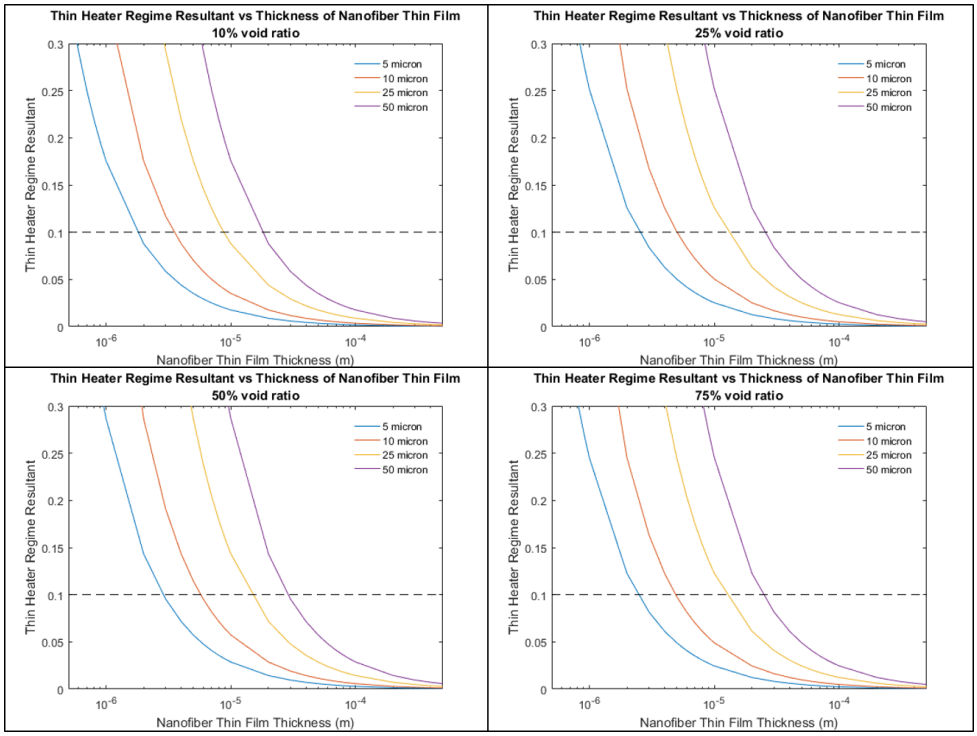

Figure 10. ω_t value at various thin film thicknesses and void percentages

Due to many of these numbers being estimates based on Eq. A.10 and averages

determined from expected thin film thickness the metal line values were chosen to be well below the 0.1 narrow heater regime distinction. Metal line widths (ω_t) of 5 μm, 10 μm, 25 μm, and 50 μm were ultimately chosen going forward in the 3ω heater design. Figure 10 demonstrates the ω_t values for each metal line thickness, demonstrating the range of nanofiber supported thin film physical properties that this measurement method will be compatible with. The physical characteristics of the nanofiber supported thin film will mostly be determined by the morphology of the nanofibers produced in the electrospinning apparatus. With the measurements available at the time of producing the metal lines, it could be said with confidence that the 3ω heaters would be able to accurately characterize the in-plane thermal conductivity of any nanofiber thin film that had a thickness greater then 2 μm as well as the cross-planer thermal conductivity of any thin film with a thickness less than 20 μm.

The eight 3ω heater geometries that were chosen were digitally produced in Solidworks, and the drawing file that contained the geometries was sent to JD Photodata for them to produce a photomask at such small geometries. The 3ω heaters were printed onto 3" silicon <100> n-type test grade wafers purchased from University Wafer.

2.2.1 Photolithography Process

Due to the incredibly small geometries being produced for the 3ω test platform all photolithography conducted in this work was completed in the University of Rhode Island's clean room. Each 3ω heater geometry was patterned onto a single silicon wafer. The wafer first goes through a prep process to ensure proper exposure to uv light during the photolithography process as well as to ensure proper adhesion of the sputtered gold material that would inevitably be deposited onto it. The first preparatory process is to clean all of the wafers in an acetone rinse and plasma

Figure 11. Plasma Cleaner used to de-scum silicon wafers

cleaner to remove any organic matter from the wafer. Each wafer is rinsed with acetone and washed additionally with methanol. The wafer is then inserted into Femto class plasma cleaner purchased form Diener, Fig 11. The plasma cleaner cleans each wafer for 30 seconds at 1 MW of power.

Following the cleaning and sterilization of the silicon wafer, each wafer is spin coated in layers of OmniCoat^{TM}purchased from MicroChem. This product acts as a sacrificial layer after the wafers are coated and exposed in SU-8 to aid in the lift off process. To ensure that the lithography process across each 3ω heater on each silicon wafer was consistent, the exact same procedure was used to best control the end product as possible. The procedure was as follows. A pre-cleaned silicon wafer is taken and centered with a spin coater. To ensure each wafer is centered as best and consistantly as possible, a small 3" diameter centering tool that contoured itself to the 3" silicon wafer as well as the vacuum chuck below it was used (Fig.

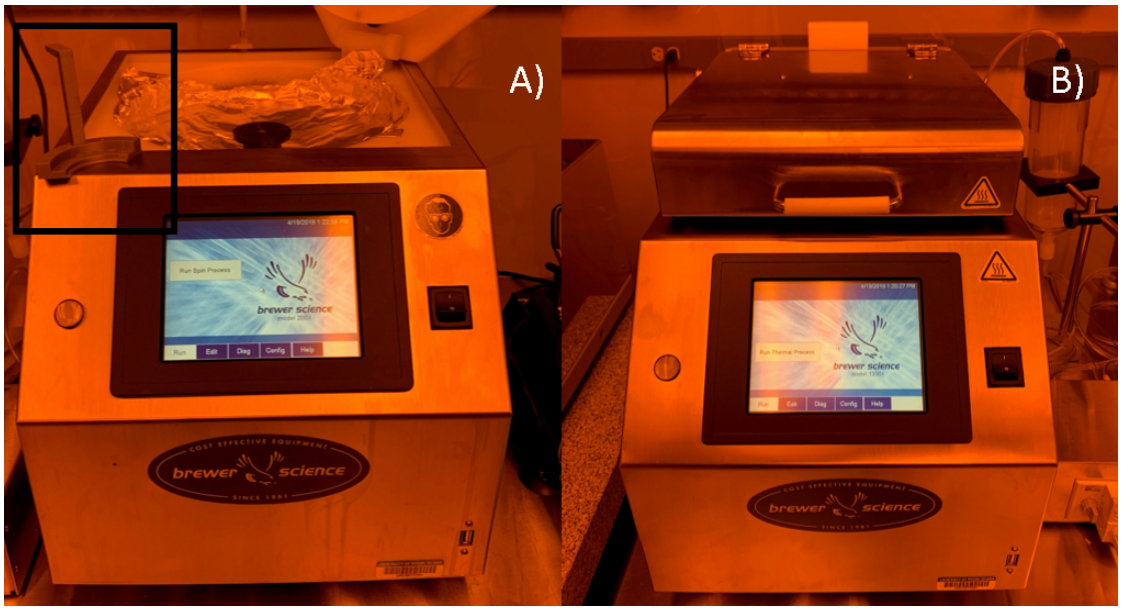

Figure 12. A) The computer controlled spin coater from Brewer Science used for spin coating the silicon wafers in this work. In the highlighted area is the 3D printed wafer centering tool used to center wafers to maximize the spin coater's effectiveness. B) The wafer oven from Brewer Science used in this work to soft bake and post exposure bake the silicon wafers.

12)A. A pipette is used to dispense 3 mL of OmniCoat^{TM}onto the center of the silicon wafer. The spin coater is loaded with a formula appropriate for the silicon wafer's size, in this case the recipe was an initial solution spreading spin off 500 RPM for 5 sec with an acceleration of 100 RPM/s. This is immediately followed by a secondary spin of 3000 RPM for 30 sec with acceleration of 300 RPM/s. The wafer is then promptly removed from the spin coater and inserted into a preheated oven held at 200° C for 1 min, Fig. 12B. The wafer is removed from the oven and allowed to cool to room temperature. According to MicroChem's data sheet on OmniCoat^{TM}, the coating should be 13 nm thick after the baking process. This process is repeated twice more to ensure a thick enough sacrificial layer of OmniCoat^{TM}. This is completed for all eight silicon wafers used to produce the 3ω heaters.

The next process is completed to apply a layer of SU-8 negative photore-

sist purchased form MicroChem and expose it to the prepared photomask. The OmniCoat^{TM}prepared silicon wafer is reinserted into the spin coater and centered. A pipette is used to dispense 3 mL of SU-8 2015 type photoresist onto the center of the wafer. The spin coater is loaded with a two step recipe starting with a solution spreading spin of 500 RPM for 10 seconds with an acceleration of 100 RPM/s. This is immediately followed by a spin of 2000 RPM for 30 seconds with an acceleration of 300 RPM/s, this rate is determined by the SU-8 data sheet depicted in Fig 13. This will result in an SU-8 layer 15 μm thick.

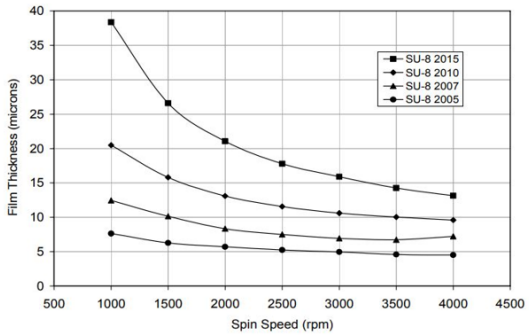

THICKNESS microns	EXPOSURE ENERGY mJ/cm^2
0.5 - 2	60 - 80
3 - 5	90 - 105
6 - 15	110 - 140
16 - 25	140 - 150
26 - 40	150 - 160

THICKNESS microns	POST EXPOSURE BAKE TIME minutes @ 95°C
0.5 - 2	1 - 2
3 - 5	2 - 3
6 - 15	3 - 4
16 - 25	4 - 5
26 - 40	5 - 6

THICKNESS microns	DEVELOPMENT TIME minutes
0.5 - 2	1
3 - 5	1
6 - 15	2 - 3
16 - 25	3 - 4
26 - 40	4 - 5

Figure 13. Condensed version of SU-8 data sheet used to produce the 3ω heaters

The coated wafer is now inserted into a pre-heated oven at 95° C for 3 minutes. To properly expose the wafer, a light test is performed on the MJB4 photomask aligner purchased from Sss Micro-technology, Fig 14, to determine the energy in mJ being output by the system. This is correlated to a necessary exposure time in seconds needed to properly expose the SU-8 coated silicon wafer. The required energy needed to properly expose the silicon wafer is again noted in Fig. 13. Fol-

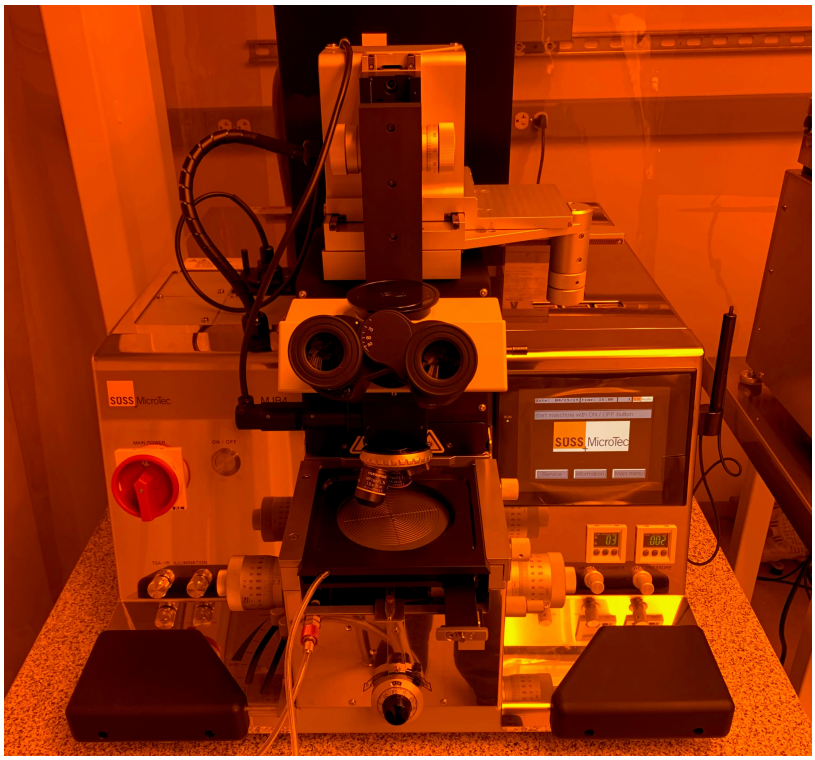

Figure 14. The MJB4 Mask Aligner purchased from Sss Micro-Technologies, used in this work.

lowing the exposure the silicon wafer is given a post exposure bake for 4 minutes at 95° C. Subsequent to the exposure process, all of the SU-8 photoresist that has been exposed to the UV light is now highly cross-linked and resistant to conventional removers. This allows for the SU-8 developer to remove all of the photoresist that was shielded from the UV light by the photomask. An OmniCoat^{TM}developer is now used to remove the now exposed OmniCoat^{TM}that was protected by the photomask, leaving the bare surface of the silicon wafer where the photomask cast its shadow during the exposure process. The process of preparing, applying, exposing, and developing the photoresist as well as the successive process of sputtering and liftoff can be observed in Fig. 15.

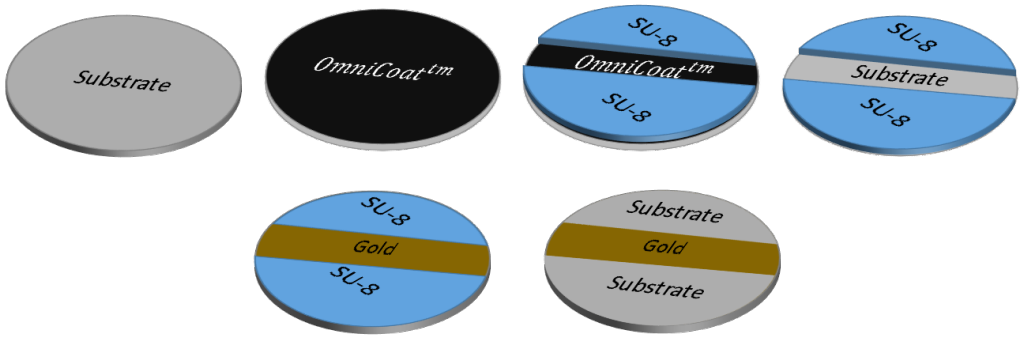

Figure 15. The development process of creating the 3ω heaters used in this work. The process as follows is, coating the substrate in OmniCoat^{TM}, coating, exposing, and developing the SU-8 with the negative photomask, developing the OmniCoat^{TM}, sputtering the 3ω heater, lift-off of the SU-8 to leave only the 3ω heater on the substrate.

2.2.2 3ω Heater Sputtering

The now exposed and developed wafers are ready to be sputtered in order to gain their metallic thin line 3ω heater. Each wafer is inserted into a sputtering system with a 4 in gold target and treated for 15 minutes. This produces a uniform coating of 200nm of gold directly onto the silicon wafer substrate, as well as the remaining cross-linked UV exposed SU-8 Photoresist. Only the gold that has adhered to the silicon wafer is needed so the rest is removed in a lift-off process. The entire silicon wafer is submerged in PG Remover purchased from MicroChem. This solution attacks and degrades the OmniCoat^{TM}sacrificial layer which sequentially removes the developed SU-8 layer that is adhered to it. The only remaining coating on the silicon wafer is the 3ω metal heater that was patterned onto the wafer through the photolithography process.

2.3 Applying the Thin Film

After creating a nanofiber thin film, for its thermal conductivity to be measured, it must be appended to a 3ω test platform. In the original 3ω procedures presented by Cahill in his original paper [12] the 3ω heater is printed directly on the

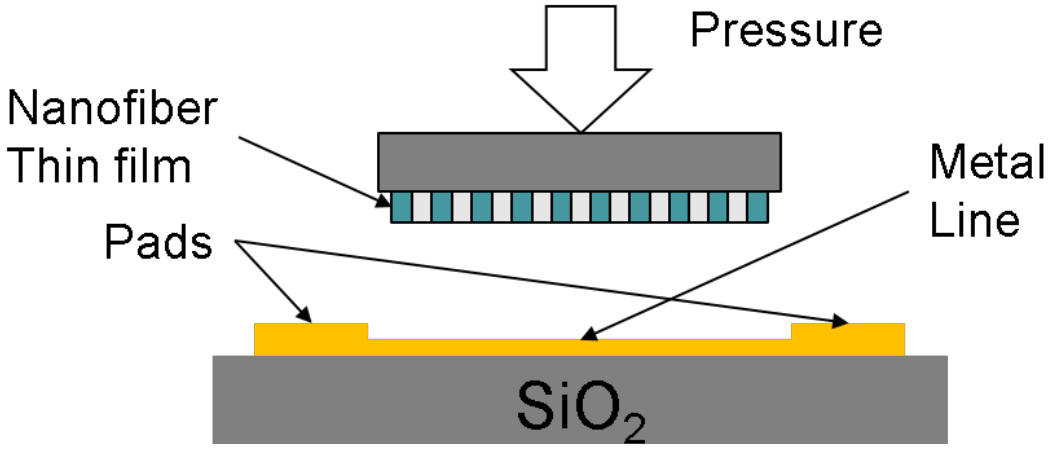

Figure 16. Attachment pressure in use to append the nanofiber thin film to the 3ω heater

test subject through photolithography. For measuring the thermal conductivity of a nanofiber supported thin film however this is not possible. Firstly the surface of a thin film is far too porous to go through any of the photolithography process, and secondly the solvents used in the photolithography process would attack and destroy the polymers used to produce the thin film. There does exist methods however of appending a sample made of porous materials to a 3ω heater produced on an appropriate medium to measure its thermal conductivity none the less [13]. In order to apply the nanofiber thin film to the 3ω heater, the thin film will be pressed onto the heater at a constant pressure. This attachment pressure will have some relation to the thermal conductivity as increasing the attachment pressure should have an inverse effect on the thermal contact resistance between the 3ω heater and the nanofiber thin film. Figure 16 demonstrates this process.

Samples are measured at various attachment pressures to allow for consistent tests at lower attachment temperatures, as when the attachment pressure reaches a critical value, the thermal conductivity test becomes a destructive test for the nanofiber samples. The nanofibers begin to lose their shape and are flattened by

the surface they are pushed against as demonstrated in Fig. 17. This plastic deformation of the nanofibers creates inconsistencies between measurements as it decreases the nanofiber film thickness at which the measurements are calibrated for and also decreases the void ratio of the nanofiber thin film. This is reflected in Eq. A.13. The attachment pressure of each nanofiber thin film is applied by the flat surface of a Standard SEM pin stub purchased from Ted Pella Microscopy. These SEM pin stubs are of standard shape and have a 12.7mm diameter as well as a 3.2mm pin. These SEM pin stubs (PELCO Tabs) are the same sample mounts used to perform the SEM microscopy of the nanofiber thin film samples as they serve both purposes equally well. The PELCO Tabs provide a flat surface that when pressed into the 3ω heater will allow to easily calculate the attachment pressure that is being applied to the nanofiber thin film sample. Under the weight of only the PELCO Tabs the nanofiber thin films will experience an attachment pressure of 6.2 Pa, the minimum attachment pressure that will be analyzed in this work.

2.4 3ω Circuit Design

For the 3ω heater to be able to conduct the experiment, it needs to have a compatible circuit designed around it. While the math and theory that determine the thermal conductivity of the nanofiber thin film sample is relatively straightforward, the output voltages from the 3ω test platform will be very low and must be compared to a reference voltage to filter out the small voltage oscillations from the general noise produced by the alternating current[12].

The circuit is arranged in a Wheatstone bridge in order to determine the non-equilibrium voltage $v_{3\omega}$. This non-equilibrium voltage is able to be compared to the input voltage of the circuit. When one side of a Wheatstone bridge is powered by a voltage supply, and the node opposite it is on a common ground to the power supply, the two remaining nodes may have their voltages compared.

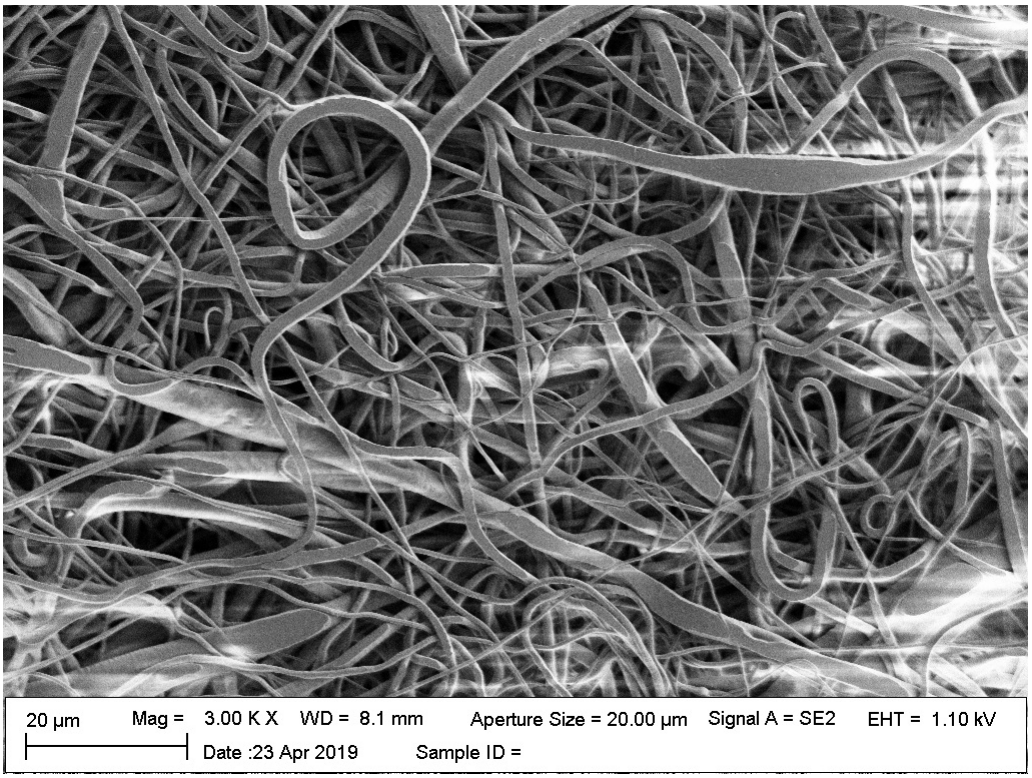

Figure 17. Randomly oriented polymer nanofibers being flattened by applied attachment pressure

For the Wheatstone Bridge to work properly both sides of it must be balanced. The Wheatstone Bridge is considered balanced when the below relation is true. This can be easily accomplished through careful selection of the resistors in the 3ω circuit, and further so by using a potentiometer for R_3 to be able to finely tune the Wheatstone Bridge. Referring to Fig. 18 the resistance of R_0 can be evaluated for all time values and represented as a function of ω through the following relation.

$$\frac{R_1}{R_0} = \frac{R_2}{R_3} \tag{6}$$

On the opposite side of this relation however, by knowing the resistance of all of the resistors in the Wheatsone bridge as well as using a known voltage input, the voltage out to the Lock-in Amplifier can be determined.

The circuit begins with an alternating current source. For this work a fre-

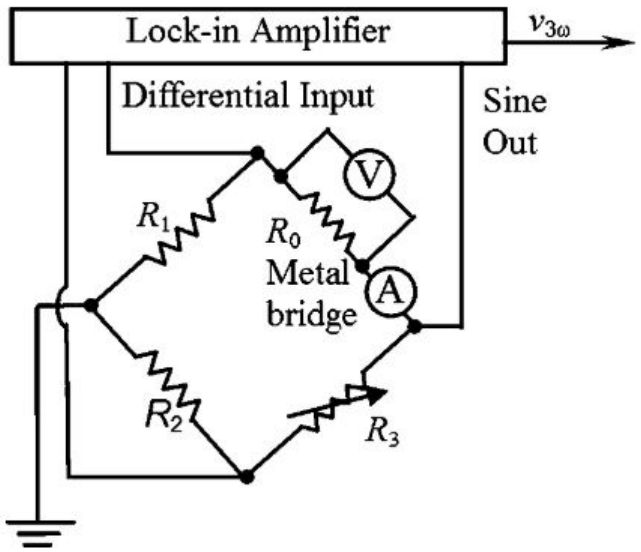

Figure 18. Schematic of the 3ω experimental circuit[13]

quency synthesizer is used to produce a sine wave. This sine wave goes in parallel to a Lock-in Amplifier to be used as a reference signal and also across the metal bridge. After going across the metal bridge the non-equilibrium voltage, $v_{3\omega}$, is also measured by the Lock-in Amplifier. This non-equilibrium voltage can be related to the 3ω voltage, $V_{3\omega}$ using the following relation made possible by the Wheatstone bridge[14].

$$V_{3\omega} = \frac{(R_0 + R_1)(R_2 + R_3)}{R_1(R_2 + R_3)} v_{3\omega} \tag{7}$$

Knowing now the 3ω voltage, the temperature relation of the thin film sample is able to be determined through the relation described by Cahill in his original work on the 3ω method [12].

$$\Delta T = 4 \frac{dT}{dR} \frac{R_0}{V} V_{3\omega} \tag{8}$$

In Cahill's original work the 3ω method is used to find the thermal conductivity of the substrate the 3ω heater is deposited on when the whole system is isolated in a vacuum chamber. Due to the modifications of this method the 3ω

heater temperature is divided by 2 because only half of the power supplied by the 3ω heater is being applied to the material of interest. The result of this assumption is:

$$\Delta T = 2\frac{dT}{dR}\frac{R_0}{V}V_{3\omega} \tag{9}$$

In this relation, V is the amplitude of the voltage sine wave applied to the 3ω heater, R_0 is the measured voltage across the 3ω heater at room temperature with no voltage oscillations, and $\frac{dT}{dR}$ is the temperature dependence of R_0. This calibration of $\frac{dT}{dR}$ is completed by measuring the temperature of the metal line at a low oscillation, and describing it as a function of the metal line's resistance.

Knowing the values of ΔT which represents the temperature oscillations of the nanofiber sample, the thermal conductivity of the sample may be determined through either a one-dimensional (1D) or two-dimensional (2D) thermal model depending on if the thickness of the metal line is much thicker than the thickness of the nanofiber thin film or is comparable to the thickness of the nanofiber thin film. Both cases are evaluated using different 3ω heaters to determine both the in-plane and cross-plane thermal conductivity of these nanofiber thin films.

List of References

[1] G. I. Taylor, "Disintegration of water drops in an electric field," *Proceedings of the Royal Society of London. Series A. Mathematical and Physical Sciences*, vol. 280, no. 1382, pp. 383–397, 1964.

[2] M. Putti, M. Simonet, R. Solberg, and G. W. Peters, "Electrospinning poly(ϵ-caprolactone) under controlled environmental conditions: Influence on fiber morphology and orientation," *Polymer (United Kingdom)*, vol. 63, pp. 189–195, 2015. [Online]. Available: http://dx.doi.org/10.1016/j.polymer.2015.03.006

[3] S. V. Fridrikh, J. H. Yu, M. P. Brenner, and G. C. Rutledge, "Controlling the Fiber Diameter during Electrospinning," *Physical Review Letters*, vol. 90, no. 14, p. 4, 2003.

[4] G. I. Taylor and M. D. V. Dyke, "Electrically driven jets," *Proceedings of the Royal Society of London. A. Mathematical and Physical Sciences*, vol. 313, no. 1515, pp. 453–475, 1969.

[5] A. L. Yarin, S. Koombhongse, and D. H. Reneker, "Bending instability in electrospinning of nanofibers," *Journal of Applied Physics*, vol. 89, no. 5, pp. 3018–3026, 2001.

[6] D. H. Reneker and A. L. Yarin, "Electrospinning jets and polymer nanofibers," *Polymers with aligned carbon nanotubes: Active composite materials*, vol. 49, no. 10, pp. 2387–2425, 2008.

[7] A. L. Yarin, W. Kataphinan, and D. H. Reneker, "Branching in electrospinning of nanofibers," *Journal of Applied Physics*, vol. 98, no. 6, 2005.

[8] A. L. Huebner and H. N. Chu, "Instability and breakup of charged liquid jets," *Journal of Fluid Mechanics*, vol. 49, no. 2, pp. 361–372, 1971.

[9] V. Thomas, M. V. Jose, S. Chowdhury, J. F. Sullivan, D. R. Dean, and Y. K. Vohra, "Mechano-morphological studies of aligned nanofibrous scaffolds of polycaprolactone fabricated by electrospinning," *Journal of Biomaterials Science, Polymer Edition*, vol. 17, no. 9, pp. 969–984, 2006.

[10] Y. Ju, K. Kurabayashi, and K. Goodson, "Thermal characterization of anisotropic thin dielectric films using harmonic joule heating," *Thin Solid Films*, vol. 339, no. 1, pp. 160 – 164, 1999.

[11] W. L. Liu, T. Borca-Tasciuc, G. Chen, J. L. Liu, and K. L. Wang, "Anisotropic thermal conductivity of ge quantum-dot and symmetrically strained si/ge superlattices," *Journal of Nanoscience and Nanotechnology*, vol. 1, no. 1, pp. 39–42, 2001.

[12] D. G. Cahill, "Thermal conductivity measurement from 30 to 750 k: the 3 method," *Review of Scientific Instruments*, vol. 61, no. 2, pp. 802–808, 1990.

[13] X. J. Hu, A. A. Padilla, J. Xu, T. S. Fisher, and K. E. Goodson, "3-Omega Measurements of Vertically Oriented Carbon Nanotubes on Silicon," *Journal of Heat Transfer*, vol. 128, no. 11, p. 1109, 2006. [Online]. Available: http://heattransfer.asmedigitalcollection.asme.org/article.aspx?articleid=1448515

[14] T. Yamane, N. Nagai, S.-i. Katayama, and M. Todoki, "Measurement of thermal conductivity of silicon dioxide thin films using a 3-omega method," *Journal of Applied Physics*, vol. 91, no. 12, pp. 9772–9776, 2002.

CHAPTER 3

Methodology and Calibration

This chapter is to review the parameters of the nanofibers produced as well as the parameters of the 3ω circuit used to measure the thermal conductivity of the nanofiber thin films. In order to conduct the experiments, first the produced nanofibers are examined under the scanning electron microscope to evaluate the size and quality of the nanofibers produced. With this information the the modeling presented in Chapter 2 can now be more accurately performed by knowing the degree of alignment as well as the void ratio of the thin film.

3.1 Nanofiber Diameter Measurements

The size of the nanofiber thin films are evaluated in the Scanning Electron Microscope in order to evaluate the size and quality of the nanofiber thin films. The scans are performed at various magnifications and electron excitations to find the appropriate measurement settings, and thin films from different electrospinning apparatus settings. In Fig. 19 the polymer nanofibers being examined were produced using the BL-TM-Pro robotic electrospinning apparatus with a solution flow rate of 9ml/hr and a voltage differential of +22kV. Two different electrospinning run times at these settings are also examined, the first for 15 minutes and the second at 45 minutes. In order to determine an appropriate nanofiber diameter distribution, each nanofiber thin film is imaged in two different locations measuring the diameter of all nanofibers that cross the horizontal mid-line of the SEM image. The first observation of these images is that the nanofibers produced span at a relatively large range of diameter sizes with this production run having the largest variation as well as having some of the largest individual fibers, with the largest being up to 1 order of magnitude larger than smallest nanofiber in the same image. With

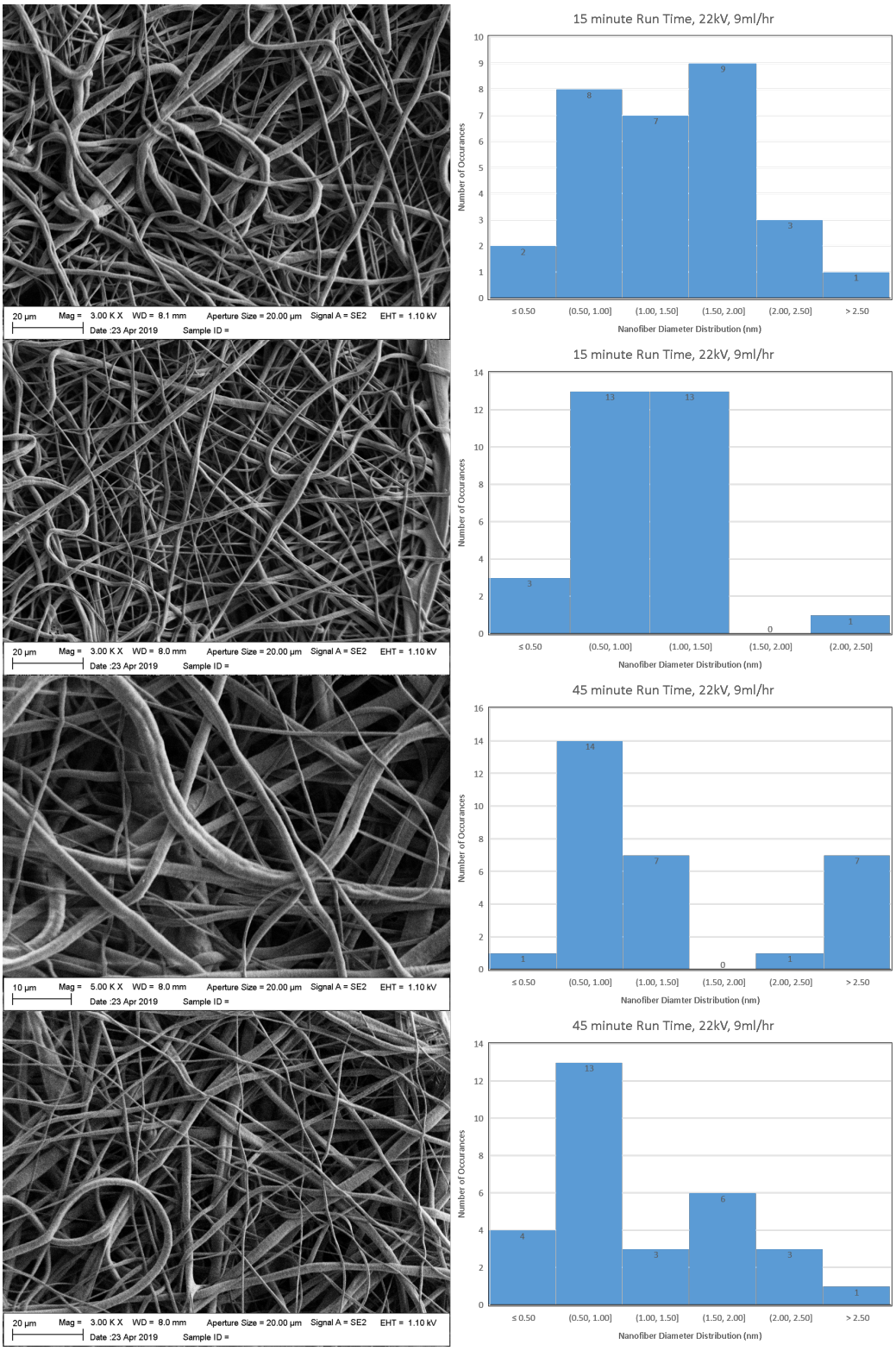

Figure 19. Distribution of nanofiber diameters when prepared at a voltage differential of +22kV and a syringe flow rate of 9ml/hr

this information, the nanofibers tend to have the highest number of occurrences in the 500 to 1000 nanometer range. The goal of this section is to determine the parameters of this individual electrospinning apparatus that will produce the most consistent nanofibers in the given machine settings. There exists many studies on relating the surface tension of the polymer solution, the solution flow rate as well as the voltage differential to the radius of the jet diameter during electrospinning [1, 2], but obtaining experimental data specific to the parameters and equipment used in this work is important in validating the models and assumptions made in this work.

Figure 20 shows polymer nanofibers produced in the same time intervals however the potential difference between the spinneret electrode and the collector was altered to +20 kV, and the flow rate remains at 9 ml/hr. These samples share a similar range of nanofiber diameters from fibers <500 nm up to 3000 nm in diameter. The difference from the original calibration production sample is that these fibers on average are smaller in diameter and have fewer occurrences of larger diameter nanofibers.

The final nanofiber diameter distribution calibration production sample was run with both a lower potential difference between the spinneret electrode and the collector as well as a lower pump rate, 20 kV and 7 ml/hr respectively. Figure 21 shows the nanofiber diameter distribution of this production run. This production run produced nanofibers with the most consistent nanofiber diameters, with a large concentration of nanobers in the 500 to 1000 nm range. All three of these production samples show randomly oriented nanofibers rather than aligned nanofibers despite being collected on a rotating drum collector. The likely cause for this is that the collector drum was rotating at a speed that caused turbulent air flow around the drum effecting the orientation of the nanofibers as they were

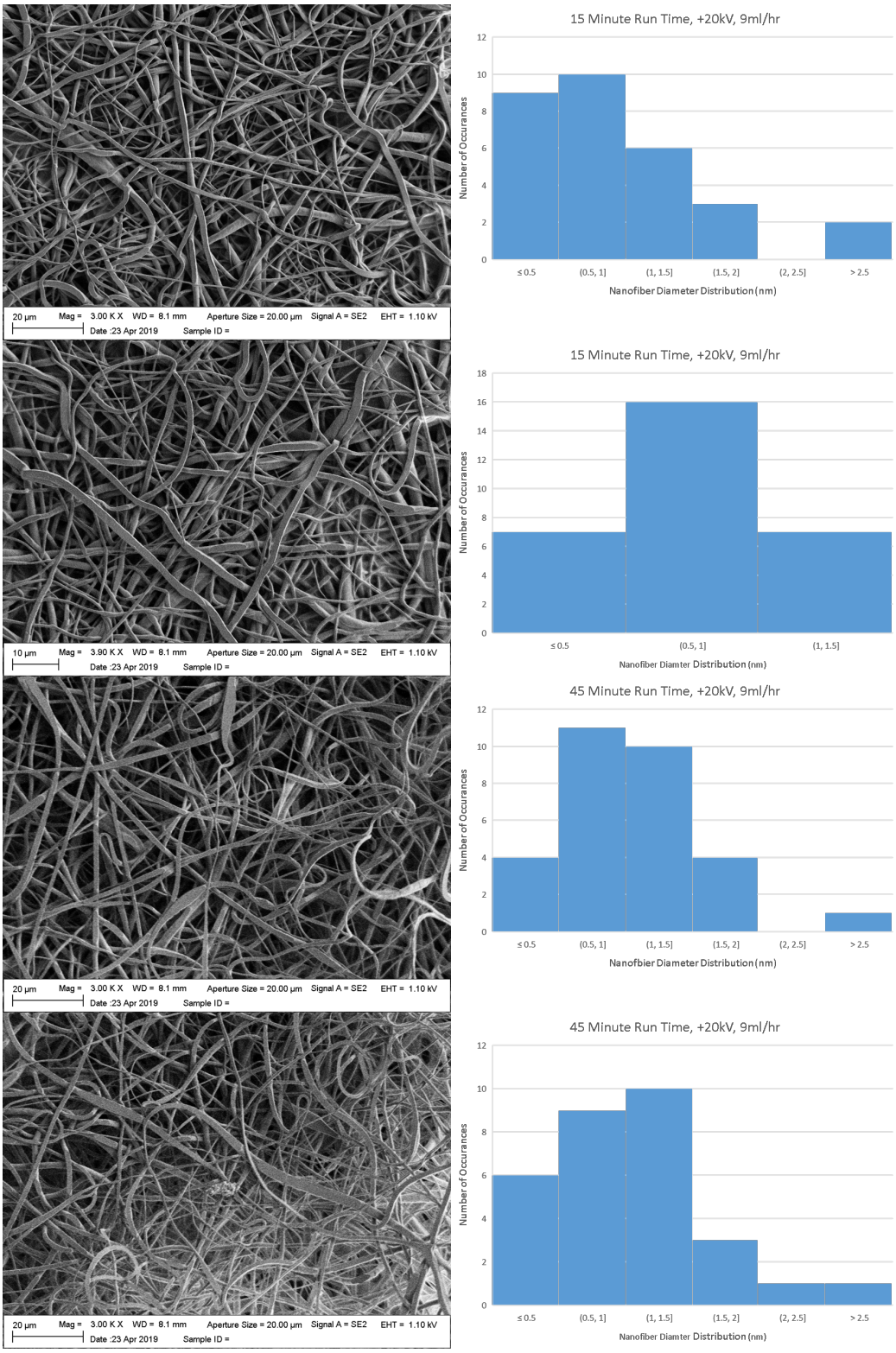

Figure 20. Distribution of nanofiber diameters when prepared at a voltage differential of +20kV and a syringe flow rate of 9ml/hr

collected on the rotating drum, but also rotating too slowly for the speed of the rotating drum to dominate the collection process and force aligned nanofibers by outpacing the turbulent air around the rotating drum. Despite the failure to produce aligned nanofibers in these production samples the measurements still prove useful in measuring the diameter distributions of the resulting nanofibers in different production parameters. In further attempts to produce aligned nanofibers the production parameters used to produce the fibers shown in Fig. 21 are used due to these production parameters having the most consistent results in the nanofiber diameter distribution. The process procedure that likely leads to this large range of nanofiber diameters is likely the concurrent use of 5 spinneret electrodes in the electrospinning apparatus. Issues such as a non-uniform distribution of electric charge among the 5 spinneret electrodes could result in more drastic fiber morphologies when compared to each other then would result if only one spinneret electrode was used. Controlling nanofiber production to narrow the nanofiber diameter distribution however is sufficient for this work as a narrow enough distribution significantly simplifies calculating the void area, which in Chapter 2 is shown to be a critical term in calculating the in-plane thermal conductivity versus the cross-plane thermal conductivity. Cross sectional area of the individual fibers is determined to be unnecessary in this calculation.

Using the results of the nanofiber morphology test outlined in this section, the parameters of the nanofiber collection method was modified in order to collect aligned nanofibers. Many papers have been published on the topic of collecting well aligned nanofibers[3, 4, 5], each with a different method of collecting the fibers to ensure their alignment. Most of these methods involve a rotating drum collector rotating at a specified linear velocity to uptake the nanofibers at a rate that ensured their alignment. The equation to determine the linear velocity of a roatating drum

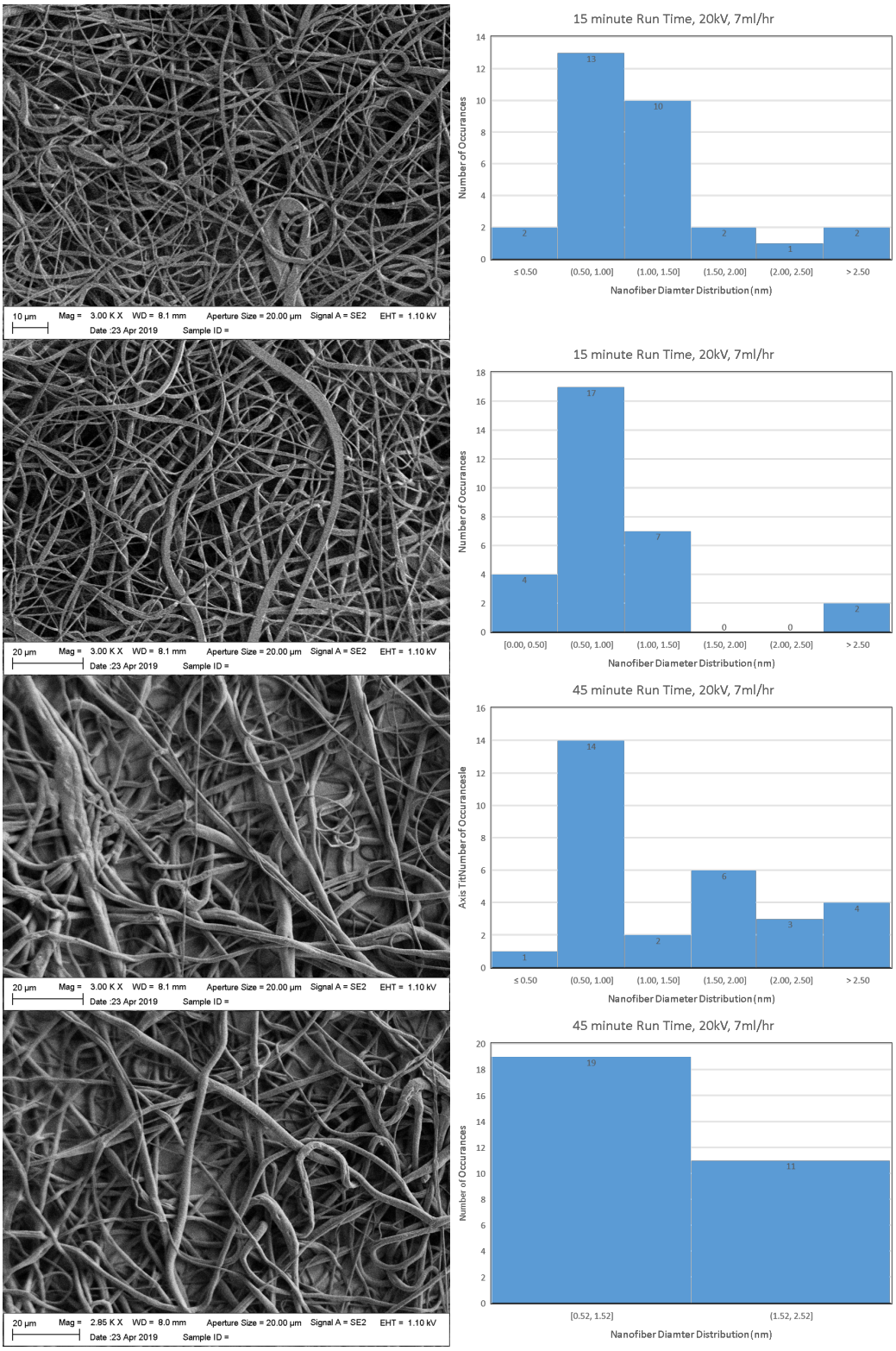

Figure 21. Distribution of nanofiber diameters when prepared at a voltage differential of +20kV and a syringe flow rate of 7ml/hr

collector based on its angular velocity is simply as follows.

$$v = r\omega \tag{10}$$

Where r is the radius of the rotating drum collector, and ω is the angular velocity of the collector. Expressing the uptake speed in linear velocity rather than angular velocity allows for the uptake speed to be simply recreated in an instance where a rotating drum collector of a different diameter is being used. In this work an uptake speed of both 1.7 m/s and 15 m/s is used in order to produce aligned nanofibers. The same acetone polymer solution was used to fabricate these nanofibers as was used in the nanofiber morphology production sample, as well as using the electrospinning parameters of a +20kV voltage differential, and a syringe flow rate of 7ml/hr. The rotating drum parameter that produced the most aligned nanofibers in this work was when set at an uptake speed of 15 m/s. At this speed all of the lower layers of nanofibers appear to be roughly in line with each other, with the top layer of the nanofibers showing some deviations. This could be for several reasons however the most likely is due to the settings of the machine as it ends its production run. At this point the drum decelerates while the syringe pump is still supplying a steady amount of solution to the charged spinneret. These fibers can be seen in Fig. 22.

Upon closer inspection of the fibers it can be seen that the fibers in the under layers of the nanofiber supported thin film show a much higher ° of alignment. This can be seen much more clearly in Fig. 23. These samples have a comparable nanofiber diameter distribution to that of the previous test so it is the sample production parameter that is selected to be used for the final thermal conductivity testing and analysis completed in this work. The nanofiber thin films are marked in such a way that they can be visibly oriented in such a way that the main direction of the fibers is in the desired direction and can be easily rotated in either direction

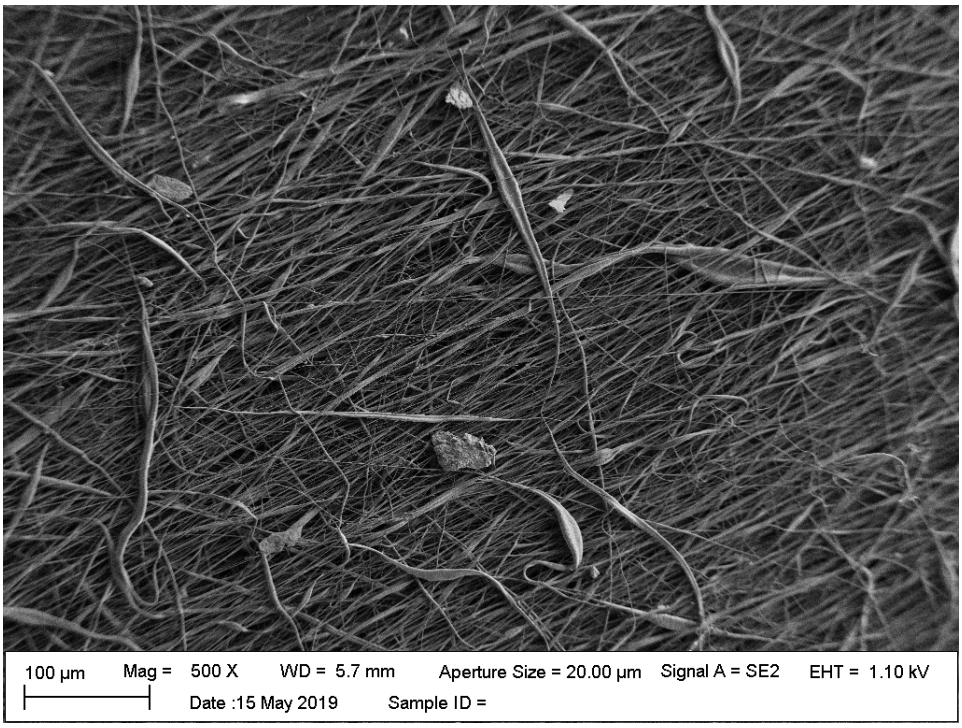

Figure 22. SEM imaging of the nanofiber produced with an uptake velocity of 15 m/s

to determine the impact of the fiber orientation on the thermal conductivity of the nanofiber supported thin film.

To determine the degree of alignment as well as the void ratio of the nanofiber thin film test samples used in this work, an imaging software tool called ImageJ is used. This software makes taking measurements such as length of fibers and their orientation easy to manage. It is also very versatile and allows for measuring the area of an image and giving a description of the area of an image whose pixels are within a certain gray-scale value. This is used to calculate the void ratio of a nanofiber thin film.

3.2 3ω Heater Resistances

The 3ω metal lines that are used in this work to determine the thermal conductivity of the polymer nanofibers are quite fragile and require care when working

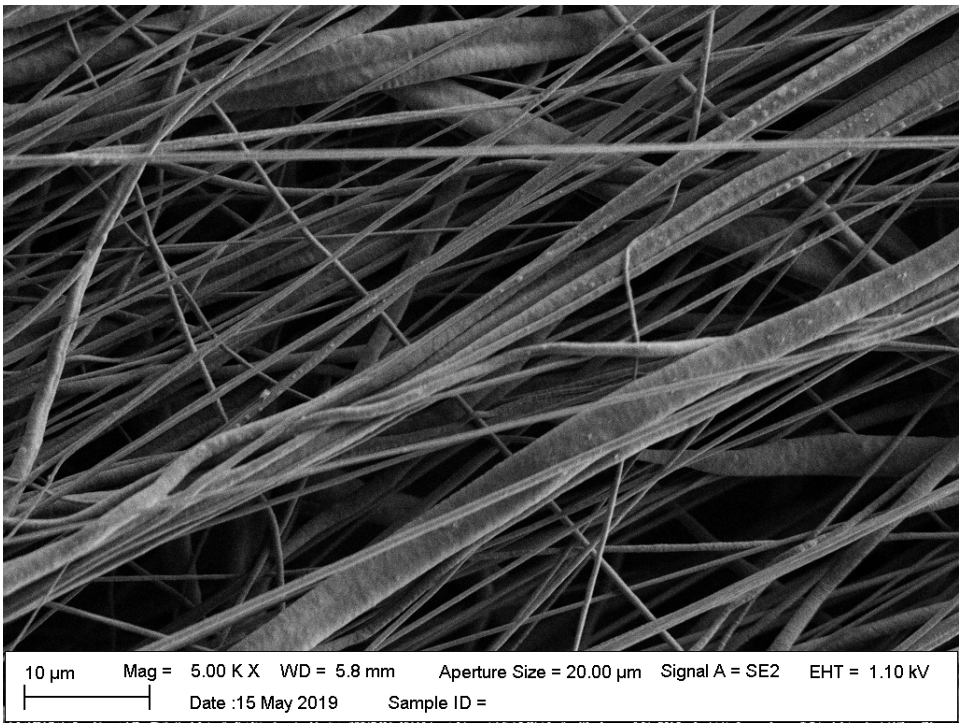

Figure 23. SEM image of the nanofiber thin film when zoomed into the nanofiber thin films under layers

with and around them. When looking to connect wires to the pads of the 3ω metal lines the first technique attempted was to solder a high gauge wire to the pad as the pads were designed to be large enough for this operation to be completed by hand. This method of attachment however failed due to the mirror finish of the silicon wafer making it impossible to bond the two metals together permanently. The second method practiced was to use thermal tape to connect the wires and the pad, however this also failed and was a destructive method as well resulting in the lift-off of the gold 3ω metal line in some cases. The final approach to attaching wire leads to the 3ω metal line pads was to use micro-manipulators. This was by far the most successful attempt at attaching the wire leads, however in some cases the copper wire was much harder than the gold that is being attached to, resulting in scratching the gold metal line. This method was used for the entirety of the work, however further techniques are explored and recommended to ensure non

destructive attachment to the metal line in a future section.

The 3ω heaters produced in this work are all produced to act as both heaters and thermometers for the samples they are measuring. In order to accomplish this they are each produced with 4 electrical pad connection terminals. One pair of the terminals is used to be integrated into the 3ω circuit while the other goes directly to the lock-in amplifier to measure the oscillating resistance and voltage drop across the 3ω heaters. When designing each 3ω heater the expected resistance of the 3ω heater was calculated using Pouillet's law.

$$R = \rho \frac{l}{A} \tag{11}$$

In this equation, R is the resistance of the 3ω heater, ρ is the material resistivity of gold, l is the length of the 3ω heater (7 mm) and A is the cross sectional area of the 3ω heater. A was calculated using the width of the selected metal line in the 3ω heater (5 μm, 10 μm, 25 μm, 50 μm) and using 200 nm as the height. The electrical resistivity of sputtered gold films has been well studied [6] and gold thin films with thicknesses above 300 Å will have the same electrical resistivity as gold in its bulk form. The silicon wafer does not contribute to the electrical resistance of the 3ω heater, as the electrical resistance per unit length of the silicon wafer is at least $\times 10^6$ that of the gold film due to the native oxide growth on the silicon wafer. The resistance of each 3ω heater is on the scale of 10's of Ohms.

When working with the 3ω method it is important to perform several measurements on the metal line to ensure that the line and equations are properly calibrated to the 3ω test platform. The first and arguably most important value to be calibrated is the temperature coefficient of resistance (α). This relation is determined using the following relation:

$$\alpha(T) = \frac{1}{R_0} \frac{dR}{dT} \tag{12}$$

In this equation, R_0 is the electrical resistance in Ohms across the 3ω metal line and dR/dT is the dependence of temperature on the electrical resistance across the metal line. This is accomplished by first measuring the electrical resistance of the 3ω metal line at what will be its normal operating temperature, and to then heat the 3ω metal line and measure the change in resistivity as the temperature rises. In order to characterize dR/dT calibration curves of each 3ω metal line used in this work must be generated. These calibration curves are generated by first placing a silicon wafer onto a hot plate and measuring the resistance between its pads. The temperature of the metal plate is raised and allowed 10 minutes to reach its new steady state. At this point the resistance of the metal line is measured again, this is completed enough times to generate a plot of the metal lines resistance over a large temperature range (x100 larger than it will experience during its normal operation) and the slope of the resulting trendline is taken. This is the dT/dR value for this metal line.

Fig. 24 is an example of the response of the 3ω metal lines resistance with increasing temperature. According to this data, α for metal line number one is -0.0091 K^{-1}. In this combination of substrates and metal line materials (Si and Au), α is negative and this is due to strain gauge effects which outpaces the thermal effect of the resistivity of a metal outlined in Eq. 11[7]. The remaining calibration lines for the 3ω heaters used in this work are represented in Fig. 25 and in Fig. 26. Figure 25 is the calibration curve for the second 10 μm metal line used in this work and it shares a very similar calibration curve to the one determined from Fig. 24, the similarities here will all likely come from both of these metal lines being prepared on the same silicon wafer. The success rate for producing the 3ω metal lines used in this work is rather low, for that reason multiple metal lines were produced on each silicon wafer to ensure the success of at least one

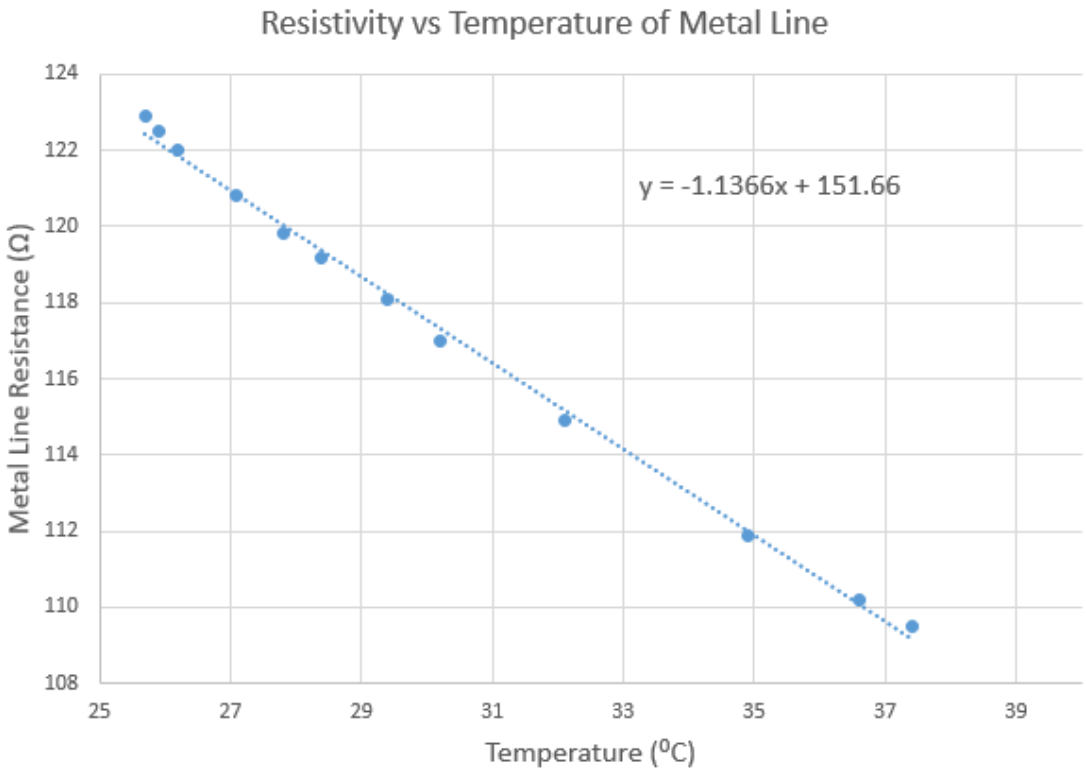

Figure 24. Resistance of the 3ω metal line vs increasing temperature

3ω metal line. The 10 μm 3ω metal line is the only metal line produced in this work in which two metal lines were acceptably prepared on the same wafer. The calibration curve represented in Fig. 26 is the calibration curve from the 5 μm metal line used in this work. This metal line has a significantly lower resistance across all temperature levels and the resistivity of this metal line displays a much less significant dependency on the temperature at which it is operating. The cause of this despite the metal line having half the smallest width of all the metal lines is its sputtered coat. This coat is much thicker than the other metal lines, however, it is still usable in this work with the generated calibration curve.

3.3 3ω Testing Procedure

With the fabricated and calibrated 3ω metal lines and 3ω circuit designed, the testing of the nanofiber thin films can be completed. To conduct the tests, an

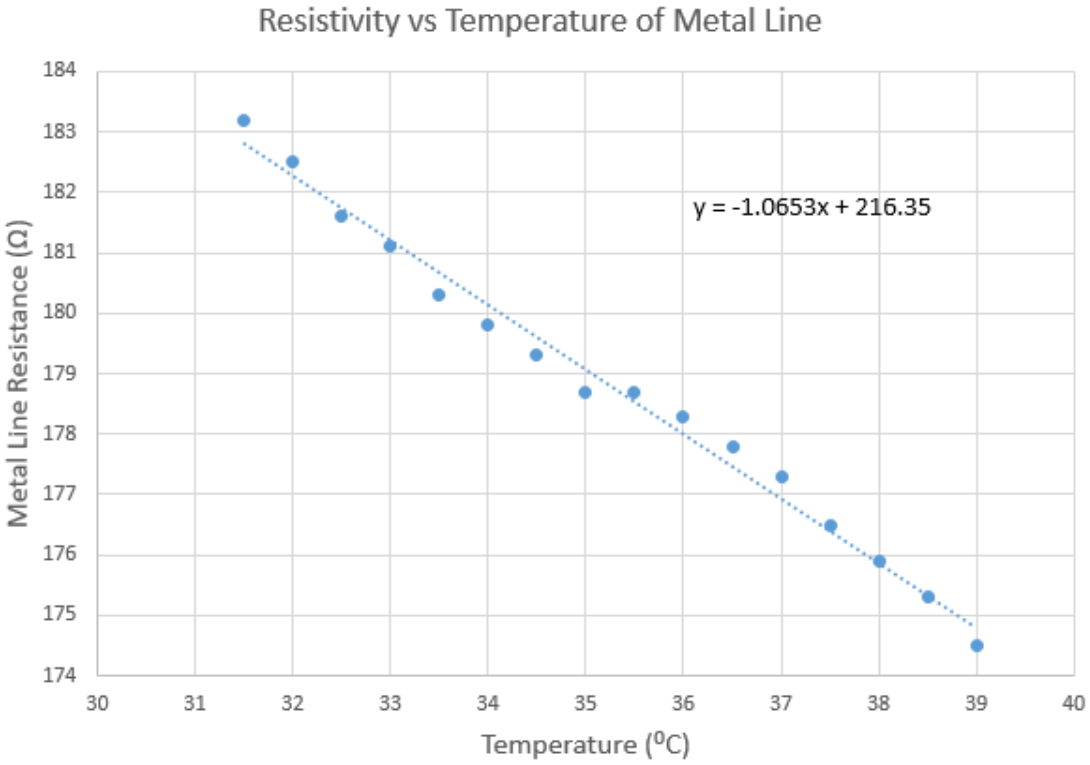

Figure 25. Calibration curve created for the second 10 μm metal line used in this work

SR530 lock-in amplifier and a Standford Research Model DS360 frequency generator is used, Fig. 29. The completed 3ω circuit is completed as it is laid out in Fig. 27. Using a 10 μm 3ω metal line the resistor and potentiometer values for the Wheatstone Bridge design are as follows.

- R_0: (3ω metal line)
- R_1: 150 Ω
- R_2: 1.5k Ω
- R_3: Balanced to Wheatstone Bridge (potentiometer)

These values are all selected around the measured resistance of the 3ω metal line, and to balance the Wheatstone Bridge designed for this experiment. Following

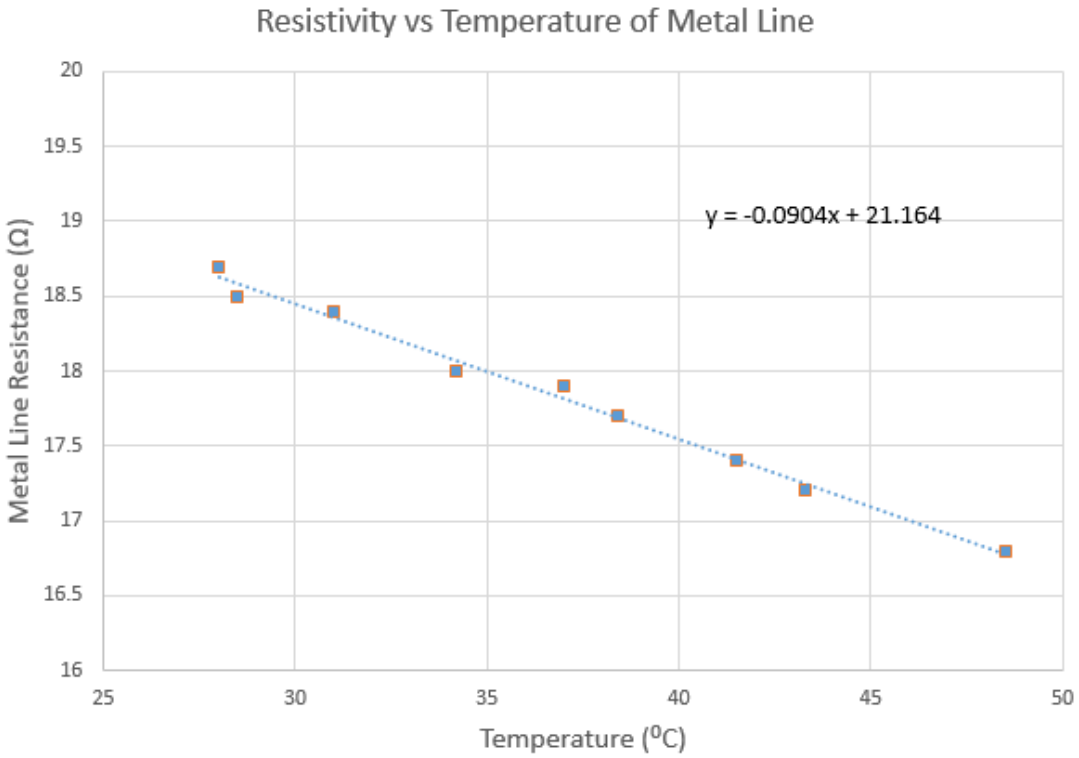

Figure 26. Calibration curve for the 5 μm metal line used in this work

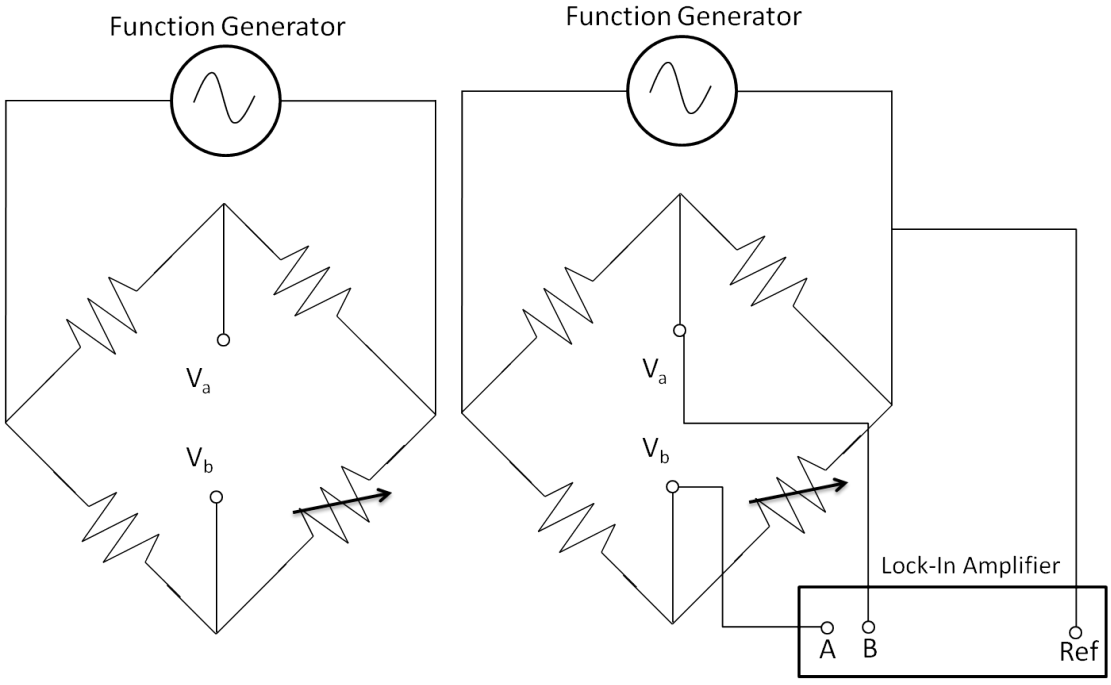

Figure 27. Wheatstone Bridge with Lock-In Amplifier plug in locations

Figure 28. The Stanford Research SR530 Lock-In Amplifier used to measure the ω voltage components of the 3ω circuits

the balancing of the Wheatstone Bridge, the A and B ports of the lock-in amplifiers are connected to the Wheatstone Bridge and the function generator is set to the desired values. The two displays of the lock-in amplifier are then observed, and R_3 is adjusted to bring the two measured voltages as close to equal as possible (this may be a simple or very delicate tuning process depending on the resolution of the used potentiometer). When the potentiometer is set, if the lock-in amplifier is not measuring equal voltage drops across the two measured nodes, the function generator can be adjusted slightly (0.1 Hz or 0.01 Hz at a time) to fully balance the bridge. Past this point the entire system is allowed two hours to reach steady state as the joule heating produced by the 3ω metal line heats the 3ω test platform. At this point the voltages measured by the lock-in amplifier are recorded and can be processed to determine the contribution of heat transfer that is conducted through the silicon wafer substrate.

The second phase of the experiment is to add the SEM pin stub that has the nanofiber thin film attached to it across the 3ω metal line. The orientation of the nanofiber thin film sample is carefully chosen in order to measure the thermal

Figure 29. The Stanford Research Model DS360 Frequency generator used to power the 3ω test platform for the test conducted in this work

conductivity of the sample in the specified orientation. The voltage differential at the measured nodes is again measured after the platform is allowed to reach steady state giving the ω voltage component of the platform with the nanofiber thin film in the attached orientation.

This process is completed again turning the nanofiber thin film 90° to now measure the thermal conductivity of the nanofiber in the opposite orientation. This entire process can be completed at as many different frequencies as needed to generate a curve that verifies the ω voltage component which is later approximated as a temperature differential and used to calculate the thermal properties of the polymer nanofiber thin film.

The final parameter to gather data for in this work is to measure the impact of the thermal contact resistance (R_c) between the polymer nanofiber thin film and the 3ω metal line. In most macroscopic systems, R_c is ignored due to its generally insignificant contribution to a system, however when working with dimensions at the scale of 100's of nanometers this loss can play a larger roll in the overall heat transfer and losses in a system. This test is conducted by running these procedures again with one distinction. The attachment pressure of the nanofiber thin film is now recorded to measure the impact it has on the calculated thermal conductivity of the polymer nanofiber thin film. The attachment pressure is measured by using

an increasing mass to push the nanofiber thin film into the 3ω heater with more force, and keeping the pressure at which it is applied constant through the use of the SEM pin mount that the nanofiber thin film is attached to.

List of References

[1] C. Thompson, G. Chase, A. Yarin, and D. Reneker, "Effects of parameters on nanofiber diameter determined from electrospinning model," *Polymer*, vol. 48, no. 23, pp. 6913 – 6922, 2007. [Online]. Available: http://www.sciencedirect.com/science/article/pii/S0032386107009275

[2] S. V. Fridrikh, J. H. Yu, M. P. Brenner, and G. C. Rutledge, "Controlling the Fiber Diameter during Electrospinning," *Physical Review Letters*, vol. 90, no. 14, p. 4, 2003.

[3] M. Putti, M. Simonet, R. Solberg, and G. W. Peters, "Electrospinning poly(ϵ-caprolactone) under controlled environmental conditions: Influence on fiber morphology and orientation," *Polymer (United Kingdom)*, vol. 63, pp. 189–195, 2015. [Online]. Available: http://dx.doi.org/10.1016/j.polymer.2015.03.006

[4] V. Thomas, M. V. Jose, S. Chowdhury, J. F. Sullivan, D. R. Dean, and Y. K. Vohra, "Mechano-morphological studies of aligned nanofibrous scaffolds of polycaprolactone fabricated by electrospinning," *Journal of Biomaterials Science, Polymer Edition*, vol. 17, no. 9, pp. 969–984, 2006.

[5] C. Y. Xu, R. Inai, M. Kotaki, and S. Ramakrishna, "Aligned biodegradable nanofibrous structure: A potential scaffold for blood vessel engineering," *Biomaterials*, vol. 25, no. 5, pp. 877–886, 2004.

[6] K. L. Chopra, L. C. Bobb, and M. H. Francombe, "Electrical resistivity of thin singlecrystal gold films," *Journal of Applied Physics*, vol. 34, no. 6, pp. 1699–1702, 1963.

[7] S. A. Putnam, D. G. Cahill, B. J. Ash, and L. S. Schadler, "High-precision thermal conductivity measurements as a probe of polymer/nanoparticle interfaces," *Journal of Applied Physics*, vol. 94, no. 10, pp. 6785–6788, 2003.

CHAPTER 4

Measurement Results and Discussion

Working with the 3ω metal heaters fabricated for this work is an incredibly delicate process. The largest portions of the 3ω metal heaters, their pads, are still at their thickest only 200 nm and without care can easily be stripped off of the silicon wafer they have been sputtered onto. The most destructive procedure of the 3ω testing however is simply attaching the wires to the 3ω metal line. The hardness of the copper wires used in this work are more than capable of scratching the surface of the gold sputtered silicon wafer, removing the coating from the wafer entirely. This can be seen in Fig. 30. The method used to attach these wire leads to the 3ω metal lines that resulted in the least amount of damage to the 3ω heater in this work has been through the use of micro-manipulators.

The micro-manipulators used in this work are Rucker & Kolls Model 221 micro-manipulators, they allowed for the precise placement of the wire leads necessary to take the voltage and current readings needed to characterize the thermal conductivity of the nanofiber supported thin films fabricated in this work. The use of these micro-manipulators did not completely solve the issue of lifting-off the gold sputtered 3ω heaters, however it did mitigate the damage and allowed testing to continue.

Conducting the experiments necessary to measure the thermal conductivity of a polymer supported nanofiber required several pieces of electronics equiptment. These pieces were borrowed from the Electrical Engineering department at the University of Rhode Island, and included a function generator as well as lock-in amplifier. The function generator was purchased from Stanford Research and the lock-in amplifier was a Stanford Research SR530 dual channel lock-in amplifier.

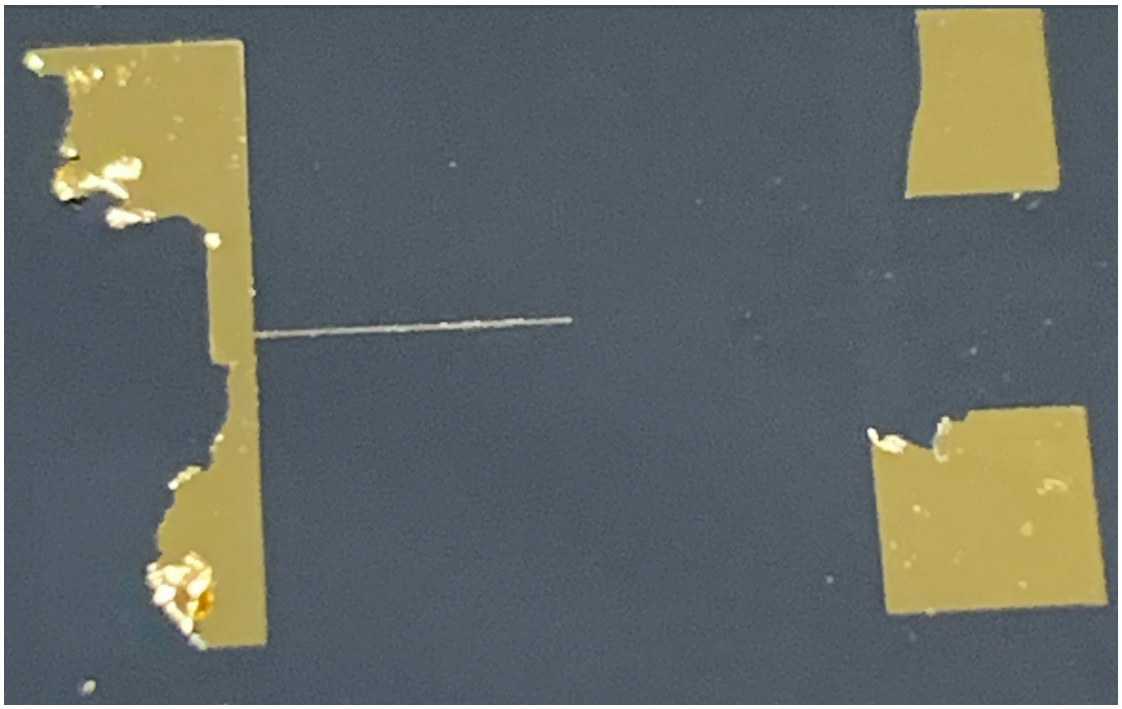

Figure 30. A 3ω heater that has been severely damaged through the normal wear that results from the 3ω testing procedures.

The function generator is set to a specific frequency and voltage. This voltage is converted to V_{rms} for all calculations in this work. This power supply is connected via BNC connectors to the reference port of the SR530 lock-in amplifier. The 3ω circuit is then further connected to a sine out port of the lock-in amplifier, this time through BNC to alligator clip connections. The positive lead of the sine out connector is connected to the node of the Wheatstone bride that is between the 3ω metal line and the potentiometer that it is in series with. The potentiometer is set to a resistance that is 10x that of the 3ω metal line. The voltages at the nodes directly after the 3ω metal line and the potentiometer are again connected to the SR 530 lock-in amplifier to determine the ω voltage component of the 3ω metal line. This is accomplished by attaching these two nodes to the A and B ports of the SR 530 lock-in amplifier. Due to the nature of this type of measurement, the 3ω circuit generates a lot of noise at various frequencies that would make simply

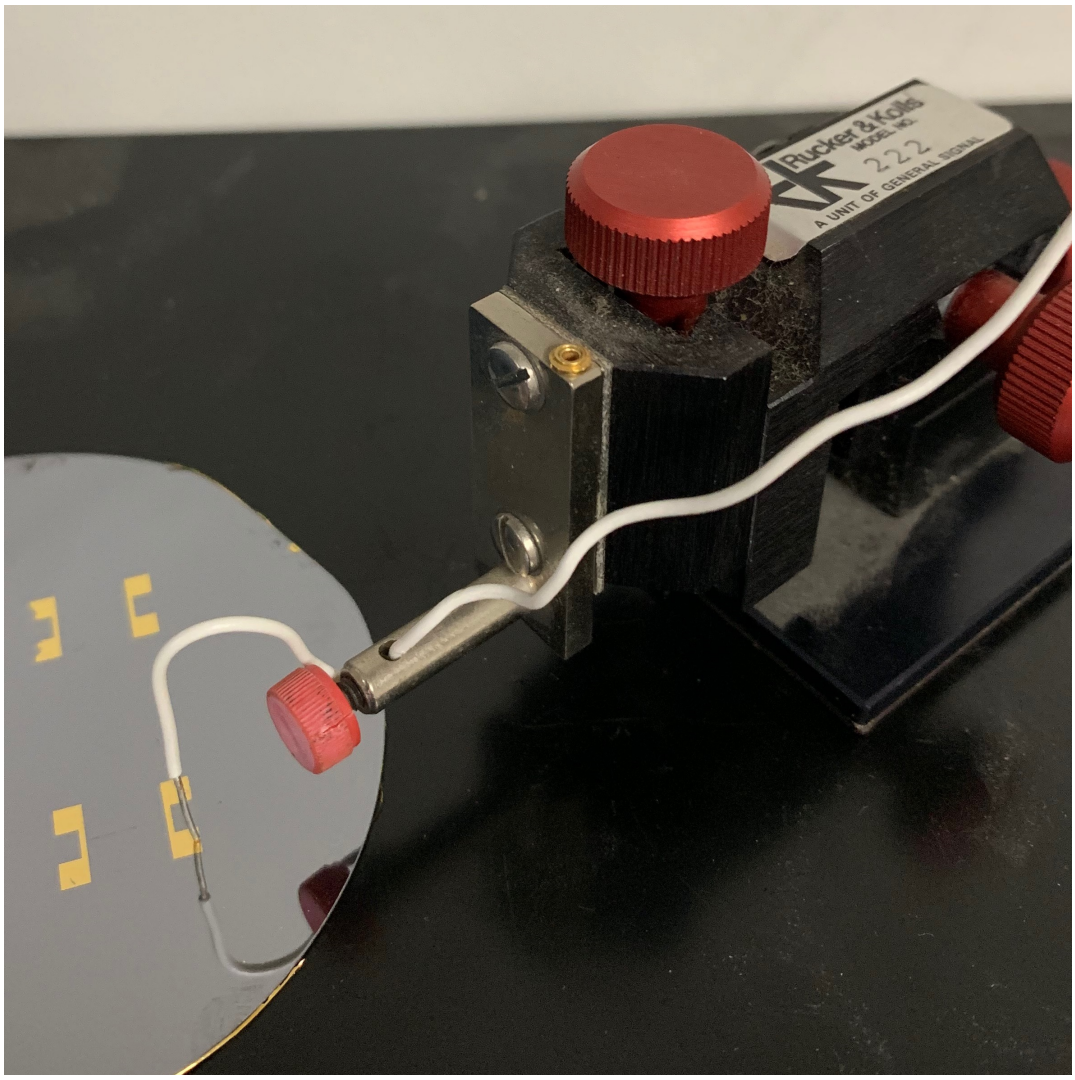

Figure 31. The Rucker & Kolls Model 221 micro-manipulators used to mitigate damage to the 3ω heaters

measuring the voltage at these nodes incredibly inaccurate. This problem is solved by the SR 530 lock-in amplifier by creating a phase-locked loop with the reference voltage that was supplied to it. This phase-locked loop will ignore all voltages that are at a frequency that does not match or is not a harmonic of the frequency supplied to the lock-in amplifier's reference port.

Through this procedure the lock-in amplifier is able to simply read the RMS voltages at the two nodes it is connected to. By subtracting these two voltages,

one is left with the ω voltage component of the 3ω metal line. This procedure is conducted twice, one with only the substrate and a second time with the thin film included. This will result in a ΔT_s for the substrate only measurement, and a ΔT_{s+f} for the substrate and nanofiber thin film measurement. The following relation is used to determine the thermal conductivity of the thin film by modifying Fourier's Law.

$$\lambda_f = \frac{Pd_f}{2b(\Delta T_{s+f}(\omega) - \Delta T_f(\omega))} \tag{13}$$

P is the electrical power put through the 3ω circuit, calculated using the rms voltage and current supplied by the function generator, and d_f is the thickness of the nanofiber supported thin film. This results in a λ_f of 4.82 $Wm^{-1}K^{-1}$ for the in planer thermal conductivity and a λ_f of 3.89 $Wm^{-1}K^{-1}$ for the cross planer thermal conductivity. Remembering that these are both effective thermal conductivities for a weighted average of the materials affected by the 3ω metal line. This shows the in-planer direction of the nanofiber supported thin film has a 20% higher thermal conductivity than the cross-planer direction. The assumption made in Chapter 2, the modeling section predicted the thermal conductivity of the in-planer direction of the nanofiber thin film to conduct 10x as much heat as the cross-planer direction of the nanofiber thin film. This calculation was performed using a model that had the individual nanofibers in the nanofiber thin film 100% parallel to one another. It is known that this was not the case for the sample tested in this work and that the nanofiber thin film was produced with nanofibers that were simply more aligned than that of a randomly oriented nanofiber thin film. The model can simply be modified to have a component that simulates non-perfectly aligned nanofibers and then predict the differences for the in-planer and cross-planer thermal conductivities.

CHAPTER 5

Summary and Future Work

5.1 Chapter Summaries

This section reviews each chapter, summarizing the methods used, results found and conclusions made as well as any relevant details of interest.

1. This chapter provides background on thermal transport at the macro and micro scale. In addition to this specific measurement techniques of the thermal conductivity measurement at the micro/nanoscale are discussed, as well as defining the proposed modifications to the 3ω method which makes this work possible.

2. This chapter looks at the results of thermally modeling a nanofiber thin film as a set of thermal resistors arranged in both series and parallel. Through this approximation it can be concluded that the axial thermal conductivity of the nanofiber thin film will be orders of magnitude greater than the trans-axial and even cross planer thermal conductivity.

3. This chapter outlines the processes and procedures used in the electrospinning process to generate the necessary fibers for this experiment, as well as outlining the process used in fabricating the 3ω heater system. Beyond just the fabrication of the 3ω heaters mentioned in this section, a process for calibrating the temperature dependance of these metal heaters is also outlined in this section.

4. Chapter 4 describes the calibration process to determine the effective morphology and allignment of the process parameters used to produce the electrospun nanofiber thin films. Along with this, the chapter goes into detail

about the material property values of the 3ω heaters and what their effects on the nanofiber thin films will be.

5. Chapter 5 describes the results found in this work using the methods, materials, and processes outlined earlier in the paper. These results are backed up by data collected over several trials with all steps used to obtain the results and all expected and possible sources of error clearly laid out.

5.2 Future Work

While the results found in this work show that the thermal conductivity of a nanofiber supported thin film is far greater than the thermal conductivity of the same polymer in bulk form, there still exists many avenues that this work can be expanded upon. The first planned extension of the work is to repeat the process again with the inclusion of metallic nanoparticles into the fiber by using a core shell spinneret, Fig. 32. Theoretically this should greatly increase the thermal conductivity of the thin film in the axial direction due to the contribution of high thermal conductivity nanoparticles. But this can be difficult to achieve experimentally. When spun in a core shell fashion nanofibers occasionally have an issue where they will form beads, creating areas in the nanofiber void of any metallic nanoparticles. The chance of this increases as the dielectric constant of the composite material also increases. This constant is likely to increase with the introduction of any metallic nanoparticles.[1, 2]. It is also likely that by using a more conductive core solution than the shell solution, it will be pulled faster and result in breakages.

The benefit to the 3ω measurement platform however is that it is applicable through a very wide range of thin film structures and varying levels of thermal conductivity measurements. What worked for the non nanoparticle infused nanofiber thin films should also work for the nanoparticle infused thin films.

Figure 32. Core-Shell Capable spinneret

In addition to testing the change in thermal conductivity of nanoparticle enhanced nanofiber thin films, there is also the goal to study the effects of creating a nanofiber thin film stack. In this work multiple nanofiber thin films would be stacked one on top of the other to reform a bulk material. The nanofiber stack would be created with up to 100 nanofiber thin films stacked one atop another. The goal of this work is to determine the thermal conductivity of the stack when the nanofibers are all oriented in the same direction, alternating perpendicularly to each other, and randomly oriented one atop another. Once again the 3ω method can be used to measure the thermal conductivity of the nanofiber stack, but in this work other methods such as parallel plate thermal conductivity testing methods will be considered.

The 3ω test platform used to measure the thermal conductivity of the polymer nanofiber thin films in this work were designed using dimensions that were shown to be successful in other works [3, 4, 5]. However they quickly failed by the mechanical lift off process that occurred during the testing portion in this work. In order to work around this, the best method that was explored was to implement the 3ω heater into a printed circuit board (pcb). By adding the entire Wheatstone bridge in Fig. 18 including a 10 turn potentiometer, the system will be made much more

robust and also be able to complete 3ω measurements without the fear of the pads being worn away. There exists additional advantages to creating a 3ω pcb platform in the form of quick connect and simplified testing procedure options being created. In the current form factor of the 3ω test platforms used in this work, the operator of the test platform must fully understand the theory behind the 3ω method, the purpose of all the electronic equipment being used in the test, how to properly operate all of the equipment, as well as connect all components of the circuit delicately to ensure proper electrical connections are made and the 3ω metal line is not damaged. In the form of a pcb with quick connect bnc connectors, all of the equipment used in this work can simply be connected and only a small amount of training would be needed to make anyone a user of this method, able to quickly and accurately collect all of the relative information from the Lock-In Amplifier, and interpret that data using the relations between resistance, ΔT and the thermal conductivity of the sample it is measuring.

List of References

[1] C. Yang, D.-G. Yu, D. Pan, X.-K. Liu, and Xia, "Electrospun ph-sensitive coreshell polymer nanocomposites fabricated using a tri-axial process," *Acta Biomaterialia*, vol. 35, pp. 77 – 86, 2016.

[2] H. Dong, V. Nyame, A. G. MacDiarmid, and W. E. Jones Jr., "Polyaniline/poly(methyl methacrylate) coaxial fibers: The fabrication and effects of the solution properties on the morphology of electrospun core fibers," *Journal of Polymer Science Part B: Polymer Physics*, vol. 42, no. 21, pp. 3934–3942, 2004.

[3] D. G. Cahill, "Thermal conductivity measurement from 30 to 750 k: the 3 method," *Review of Scientific Instruments*, vol. 61, no. 2, pp. 802–808, 1990.

[4] X. J. Hu, A. A. Padilla, J. Xu, T. S. Fisher, and K. E. Goodson, "3-Omega Measurements of Vertically Oriented Carbon Nanotubes on Silicon," *Journal of Heat Transfer*, vol. 128, no. 11, p. 1109, 2006. [Online]. Available: http://heattransfer.asmedigitalcollection.asme.org/article.aspx?articleid=1448515

[5] T. Yamane, N. Nagai, S.-i. Katayama, and M. Todoki, "Measurement of thermal conductivity of silicon dioxide thin films using a 3-omega method," *Journal of Applied Physics*, vol. 91, no. 12, pp. 9772–9776, 2002.

APPENDIX

Design and Modeling

A.1 Energy Balance

To start analyzing the thermal conductivity of the nanofibers, the energy balance equation must first be used and solved with the models boundary problems to identify important terms.

$$\frac{(\partial^2 T)}{(\partial x^2)} + \frac{(\partial^2 T)}{(\partial y^2)} + \frac{(\partial^2 T)}{(\partial z^2)} + \frac{q'}{k} = 0 \tag{A.1}$$

Because the heat transfer is unidirectional and there is no internal heat generation, the equation simplifies to the following:

$$\frac{(\partial^2 T)}{(\partial x^2)} = 0 \tag{A.2}$$

The variables can further be non-dimensionalized

$$\theta = \frac{T - T_l}{T_l - T_h} \tag{A.3}$$

$$X = \frac{x}{l} \tag{A.4}$$

Defining the boundaries of the system allows for the differential equation to be solved for all values within the boundaries, thus:

$$\begin{aligned} T = T_L = \theta_L \\ T = T_H = \theta_H \end{aligned} \tag{A.5}$$

$$\begin{aligned} @x = 0; X = 0 \\ @x = L; X = L \end{aligned} \tag{A.6}$$

Differentiating with respect to these variables as well as applying the boundary conditions results in the following temperature relationship

$$\theta = (\theta_H - \theta_L)X \tag{A.7}$$

This temperature relationship can be used in the Fourier Equation to define the heat flux through the material at its steady state. Looking at the terms that have an effect on the total heat flux through the material, keeping the temperature sources and the distance constant, only the effective thermal conductivity of the nanofiber thin film can be changed to effect the heat flux.

$$q'' = -k\frac{\partial\theta}{\partial x} \tag{A.8}$$

$$q'' = -\frac{k}{l}(\theta_H - \theta_L) \tag{A.9}$$

A.2 Thermal Resistivity Model

To compare the cross-plane thermal conductivity (λ_x) and the in-plane thermal conductivity (λ_y) a thermal resistor model can be analyzed. The thermal resistance of a material or composite is described as being directly proportional to the distance between the high temperature (T_H) and low temperature (T_L) sources, and inversely proportional to the cross sectional area (A) and effective thermal conductivity per unit length (k_{eff}) of the material. Of these terms the effective thermal conductivity is the most important term as it is dependent on the temperature differential being oriented in the trans-axial direction of the nanofiber thin film, or oriented in the axial direction of the nanofiber thin film.

$$R = \frac{\Delta x}{k_{eff}A} \tag{A.10}$$

To define k_{eff} the thermal conductivity of both the nanofiber and the void between them as well as a ratio of void to nanofiber volume is needed. These terms are defined as k_f, k_a, and ϕ for the thermal conductivity of the fiber, thermal conductivity of air, and void percentage respectively. Inserting these into equation A.10 for the axial case seen in Fig. A.1A and the trans-axial case seen in Fig. A.1B results in a thermal resistance in the axial direction ($R_\parallel$), and a thermal resistance in the trans-axial direction ($R_\perp$).

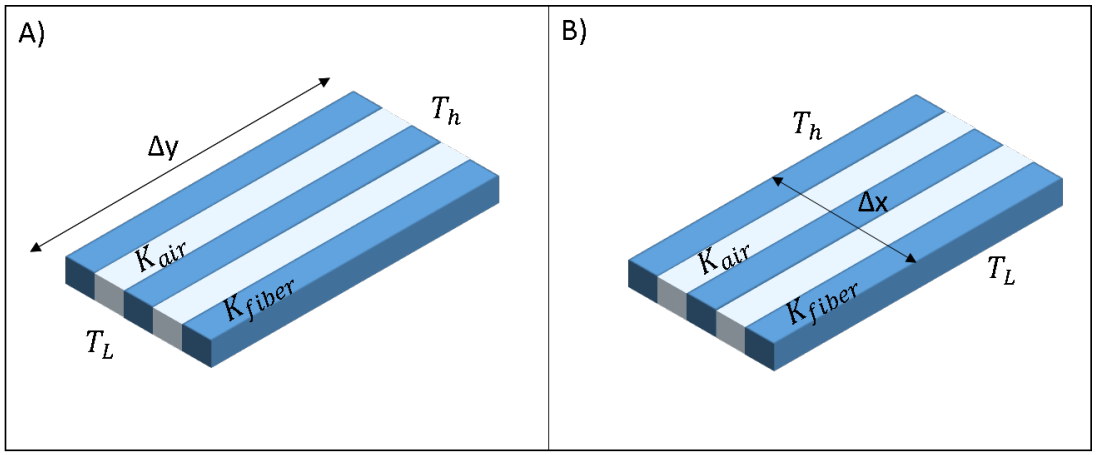

Figure A.1. A) Model of materials acting as thermal resistors in parallel for when the temperature differential is applied axially to the thin film. B) Model of materials acting as thermal resistors in serial for when the temperature differential is applied trans-axially.

$$R_{\parallel} = \frac{\Delta y}{(k_f(1-\phi) + k_a\phi)A} \tag{A.11}$$

$$R_{\perp} = \frac{\Delta x}{k_a\phi A} + \frac{\Delta x}{k_f(1-\phi)A} \tag{A.12}$$

If Δy and Δx are assumed to be equal, Eq. A.11 can be divided by Eq. A.12 to create a relation between the thermal resistance of a well aligned composite material thin film in its axial and trans-axial directions.

$$R_{\parallel} = R_{\perp}\frac{k_f k_a(1-\phi)\phi}{(k_a(1-\phi) - k_f)^2} \tag{A.13}$$

This relationship shows that the resistance in the axial direction will reduce rapidly in comparison to the trans-axial thermal resistance with increasing k_f. Most notably in this relation however is that the cross-sectional area term, A, has no effect when comparing the two thermal resistances. This shows that it is not dependent on how many or how thick the fibers are, but only the fraction of the thin film that is fiber or air.

A.3 3ω Thermal Calculations

The 3ω heaters are responsible for determining the thermal characteristics of the measured polymer thin films. This is completed by integrating the 3ω test platform into a specialized circuit. This circuit contains a reference current, whose current is the same as the 3ω input current, and a Wheatstone bridge to balance the circuit and determine the difference between the 3ω signal and the reference signal. The reference current is provided by a signal generator. This signal generator is able to have the frequency of the given signal modulated as needed to provide signals at various voltages and frequencies. Thermal conductivity measurements are typically conducted by comparing the differences in a sample's reaction to a signal given at two different frequencies, f_1 and f_2. All voltages applied in this work are RMS voltages.

$$V_{rms} = \frac{V_{Peak}}{\sqrt{2}} \tag{A.14}$$

The thermal conductivity of a nanofiber thin film is first measured as a change in temperature of the sample, ΔT caused by the oscillating joule heating exerted on the sample by the 3ω heater. This is described by the following relation.

$$\Delta T = 4\frac{dT}{dR}\frac{R}{V}V_3 \tag{A.15}$$

In this relation, $\frac{dT}{dR}$ is the differentiated calibration of the metal line, R is the average resistance of the 3ω heater, V is the V_{RMS} of the input signal into the 3ω heater, and V_3 is the voltage differential across the 3ω heater. V_3 is evaluated at two different frequencies in order to determine the thermal conductivity of the measured sample. The thermal conductivity of the nanofiber thin film can be found through the following relation[1].

$$\Lambda = \frac{V^3 ln(f_2/f_1)}{4\pi l R^2 (V_{3,1} - V_{3,2})}\frac{dR}{dT} \tag{A.16}$$

In this equation, $V_{3,1}$ is the 3ω voltage at frequency f_1 and $V_{3,2}$ is the 3ω voltage at frequency f_2, and l is the length of the 3ω heater.

A.4 Thermal Circuit For In-Plane and Cross-Plane Heating

The heat conduction experienced when heating a nanofiber thin film can be modeled as a thermal circuit. The power input is represented by P'' with half of the energy going into the silicon wafer that the 3ω heater is deposited onto and the other half going into the polymer nanofiber on top of it. The steady-state heat conduction for this situation in the frequency domain is expressed as:

$$\frac{d^2\Delta T(x,\omega)}{dx^2} = a^2\Delta T(x,\omega) \tag{A.17}$$

when considering the following boundary conditions at x = 0 (the center point of the 3ω heater):

$$-k\frac{d\Delta T(x,\omega)}{dx} \tag{A.18}$$

$$\Delta T(l,\omega) = 0 \tag{A.19}$$

in this expression $a = \sqrt{j\omega\rho c/k}$. j is the imaginary component of an alternating current, ρ is the material density, c is the specific heat, k is the thermal conductivity, and l is the thickness of the medium. P'' represents the power applied, and ω is the angular frequency. The temperature variation with respect to the input frequency is described as:

$$\Delta T(\omega) = \frac{P''tanh(al)}{ak} \tag{A.20}$$

Thermal impedence may then be determined by dividing Eq. A.20 by P'' resulting in [2]:

$$Z(\omega) = \frac{tanh(al)}{ak} \tag{A.21}$$

From the definition of electrical impedance, thermal impedance can also be inferred through its relation to the thermal resistance, thermal capacitance, and the input

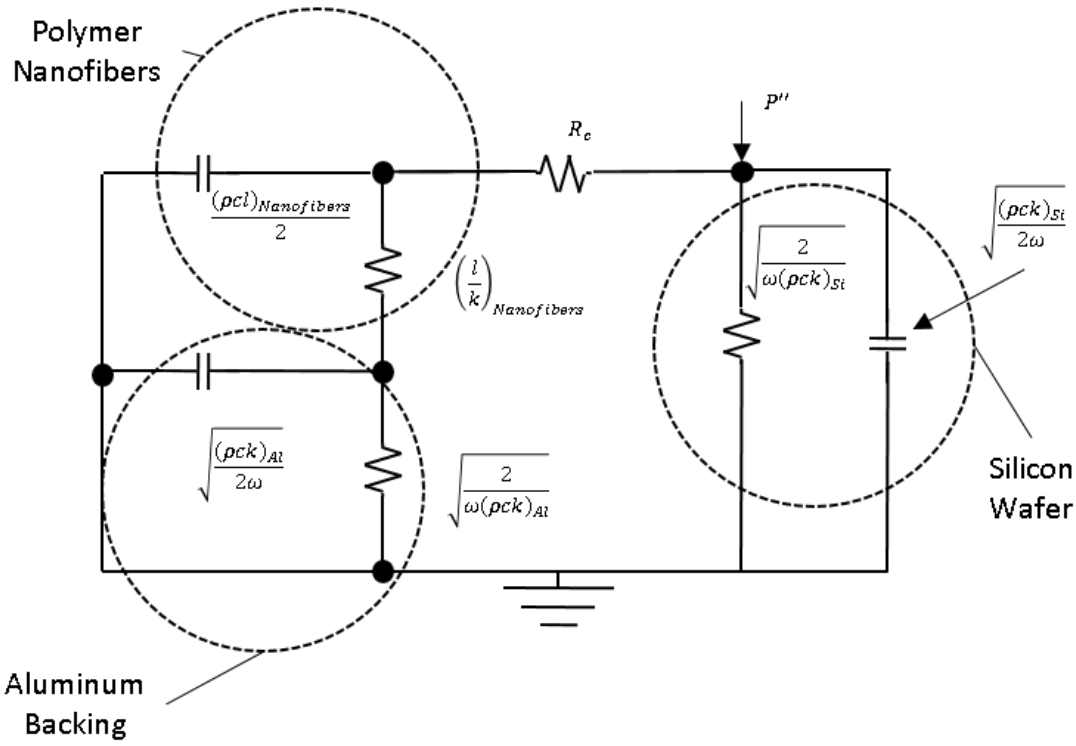

Figure A.2. Thermal Circuit equivalent for cross-planer heating

frequency.

$$Z^{-1}(\omega) = R^{-1} + j\omega C \tag{A.22}$$

A.4.1 Thermal Circuit in Cross-Planer Heating

As seen in Fig. A.2 the first loss encountered by the power supplied by the 3ω heater is the contact resistance between the resistor and the polymer nanofibers. In most situations the contact resistance between two materials is ignored because it is of a much smaller magnitude then all other equivalent resistances. This is the case between the 3ω heater and the silicon wafer as the heater is well applied to the silicon wafer. The contact resistance in this circuit is not known, but the variation in contact resistance will be explained through the use of varying attachment pressures used to force the polymer nanofibers into the 3ω heater. Previous work

has shown an inverse relationship between the attachment pressure of a specimen and the thermal contact resistance when using the 3ω method [2]. In the case of cross-planer heating the thermal resistance expression for the nanofibers and the aluminum backing are different because the polymer nanofibers are a normal material in heat transfer and the aluminum backing is considered a semi-infinite medium. This leaves the thermal resistance for the polymer nanofibers as:

$$R = \frac{l}{k} \tag{A.23}$$

leaving the thermal capacitance to be described as:

$$C = \frac{\rho c l}{2} \tag{A.24}$$

When taking into account the assumption that there is no longer a ΔT across the entirety of the medium (The temperature distribution of the medium has some points with $T{=}T_\infty$) the medium can be considered semi-infinite. As this happens al goes sufficiently to ∞ for the case $tanh(al) = 1$. In this case Eq. A.22 is used to determine the thermal resistance and thermal capacitance of both the aluminum backing of the polymer nanofibers and the silicon wafer. The result of this is:

$$R = \sqrt{\frac{2}{(\omega \rho c k)}} \tag{A.25}$$

$$C = \sqrt{\frac{\rho c k}{2\omega}} \tag{A.26}$$

In this case the equivalent thermal impedance of the thermal circuit can be determined simply by using the equivalent resistance equation.

$$\frac{1}{Z_t(\omega)} = \frac{1}{1 + [(R_{Nnfbs} + Z_{Al}(\omega))^{-1} + j\omega C_{Nnfbs}]} + \frac{1}{Z_{Si}(\omega)} \tag{A.27}$$

This equivalent thermal impedance is further inserted into Eq. A.20 to result in:

$$\Delta T = P'' Z_t(\omega) \tag{A.28}$$

Using the ΔT obtained from previous equations on the 3ω method, the non-negligible contact resistance between the polymer nanofibers and the 3ω heater can now be evaluated and further be related to its attachment pressure to determine the relation there.

A.4.2 Thermal Circuit for In-Planer Heating

When using a 3ω heater that produces purely in-planer heating the thermal circuit simplifies to totally exclude the aluminum backing. In this scenario the polymer nanofibers are now assumed to be a semi-infinite medium. With this assumption not enough energy penetrates into the polymer nanofibers to reach the aluminum backing as the temperature distribution equals the ambient temperature at the edges of the polymer nanofiber thin film. As is seen in Fig. A.3 the thermal circuit simplifies to include only the thermal resistance of the silicon wafer, the polymer nanofiber thin film, and the contact resistance between the medium and the 3ω heater, as well as the thermal capacitance of the silicon wafer and the polymer nanofiber thin film. The relation in this case for the thermal contact resistance between the polymer nanofiber thin film and the 3ω heater changes little. It is now simply determined through the thermal impedance of the two mediums in parallel rather than 3 mediums in a complex circuit. The thermal resistance for both the polymer nanofiber thin film as well as the silicon wafer in this configuration can be determined using Eq. A.25, and the thermal capacitance is determined using Eq. A.26. The reason why the polymer nanofibers can be considered a semi-infinite medium in this situation goes back to the relation $tanh(al)$. With a being directly related to the input frequency supplied by the frequency synthesizer and l being the thickness of the medium (polymer nanofiber thin film in this case), using a higher input frequency as well as a thicker polymer nanofiber thin film, $tanh(al) \rightarrow 1$.

In order to calculate the thermal contact resistance when using an in-plane

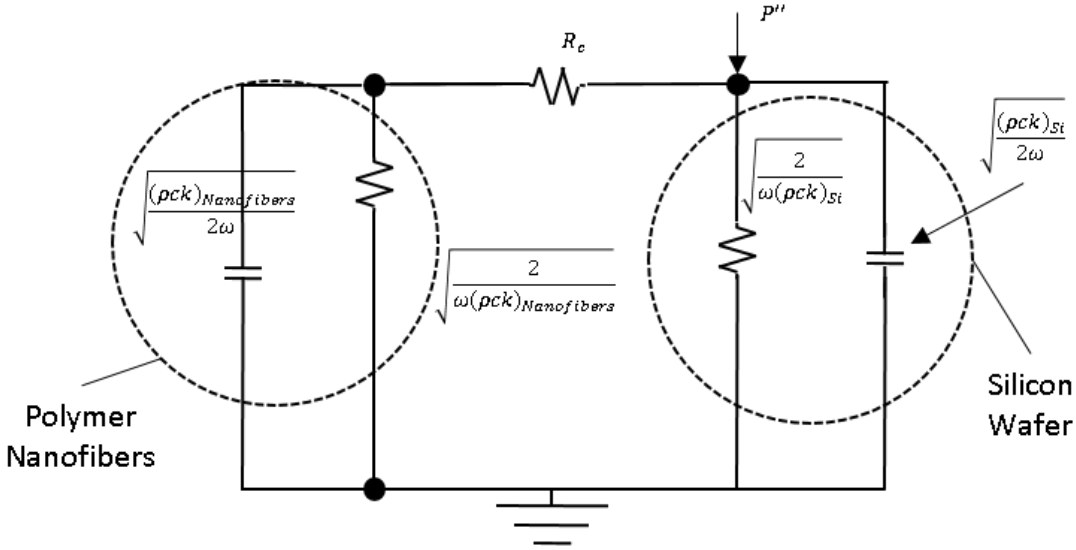

Figure A.3. Thermal circuit equivalent for in-planer heating

heating configuration the ΔT must first be determined using methods discussed earlier in this work, and relating it to Eq. A.28. However for this scenario $Z_t(\omega)$ is found using a different relation than used in the cross-planer heating scenario. To find $Z_t(\omega)$ in this scenario the following relation is used.

$$\frac{1}{Z_t(\omega)} = \frac{1}{R_c + Z_{pcl}} + \frac{1}{Z_{Si}(\omega)} \tag{A.29}$$

where Z_{pcl} can be found calculated as the inverse of the thermal resistance of the polymer nanofiber thin film plus the product of the complex conjugate times the thermal capacitance of the polymer nanofiber thin film.

$$Z_{pcl}^{-1} = R_{pcl}^{-1} + j\omega C_{pcl} \tag{A.30}$$

Using the same methods to calculate the thermal contact resistance found in the previous section, the thermal contact resistance between the 3ω heater and the polymer nanofiber thin film can also be analytically determined.

As seen in both the in-planer and cross-planer thermal circuit, the thermal inertia of the mediums through which heat is transferred plays a significant roll.

The thermal inertia of a material is defined as follows.

$$I = \sqrt{\rho c k} \tag{A.31}$$

I, however is not included in the thermal circuit approximations as it could easily be confused with current. All calculations using the thermal conductivity of the mediums in this work were used using their values at an ambient temperature of 24.0 °C. This was particularly important for the thermal values of the silicon wafers used in this work as the thermal properties of silicon vary significantly with temperature [3].

List of References

[1] D. G. Cahill and R. O. Pohl, "Thermal conductivity of amorphous solids above the plateau," *Phys. Rev. B*, vol. 35, pp. 4067–4073, Mar 1987.

[2] X. J. Hu, A. A. Padilla, J. Xu, T. S. Fisher, and K. E. Goodson, "3-Omega Measurements of Vertically Oriented Carbon Nanotubes on Silicon," *Journal of Heat Transfer*, vol. 128, no. 11, p. 1109, 2006. [Online]. Available: http://heattransfer.asmedigitalcollection.asme.org/article.aspx?articleid=1448515

[3] G. A. Slack and C. J. Glassbrenner, "Thermal conductivity of Si and Ge from 3K to the melting point," *Physical Review*, vol. 1431, 1964. [Online]. Available: https://journals.aps.org/pr/pdf/10.1103/PhysRev.134.A1058

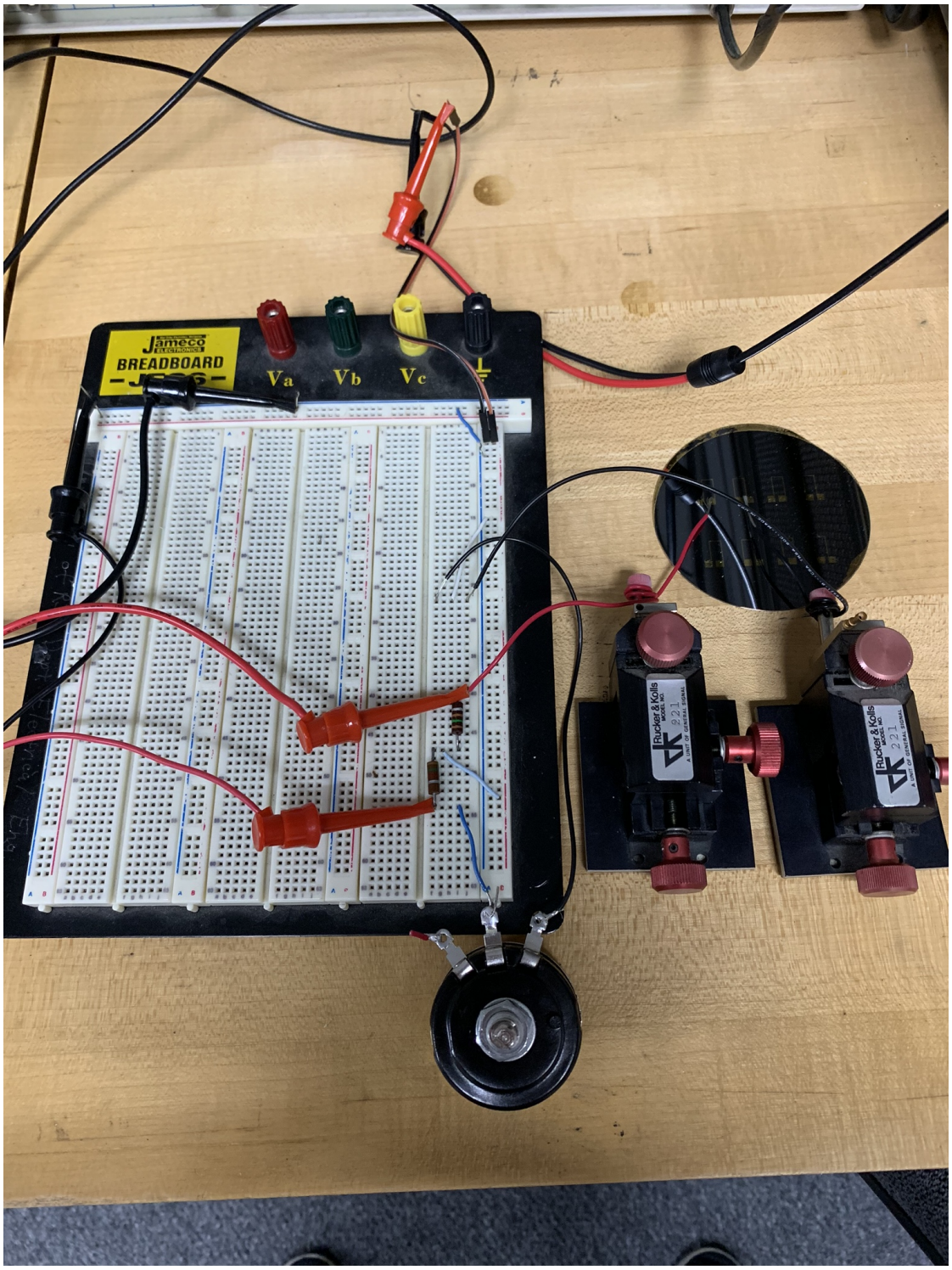

Figure A.4. Overhead view of the breadboard and final full setup of the 3ω circuit board design

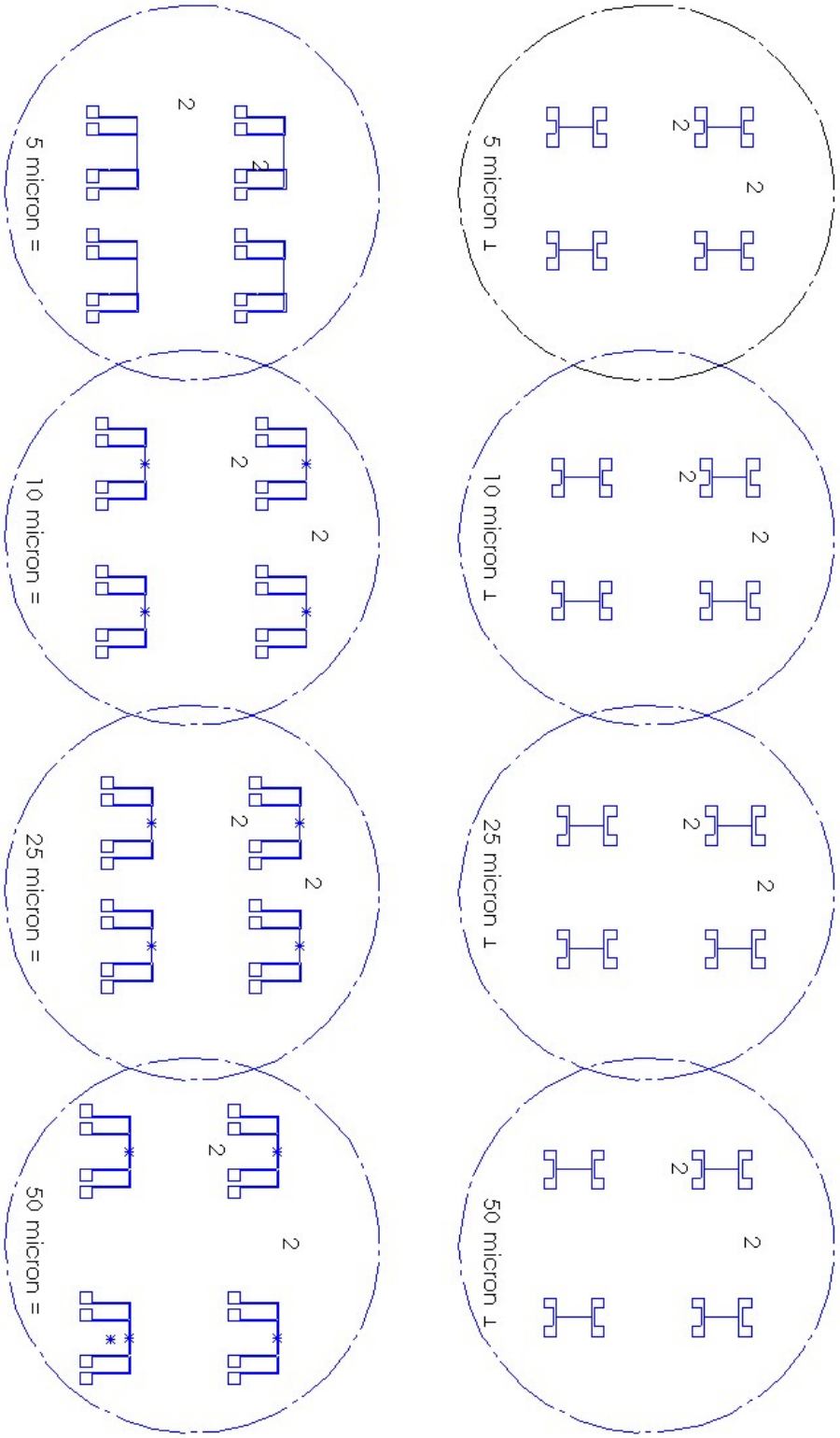

Figure A.5. Full drawing file of 3ω heaters used

BIBLIOGRAPHY

AL-KHUDARY, N., "Material thermal conductivity mesurement by the 3-omega method application to polymer characterization using inkjet printing technology," *These*, p. 264, 2014.

Bhattarai, N., Edmondson, D., Veiseh, O., Matsen, F. A., and Zhang, M., "Electrospun chitosan-based nanofibers and their cellular compatibility," *Biomaterials*, vol. 26, no. 31, pp. 6176–6184, 2005.

Cahill, D. G., "Thermal conductivity measurement from 30 to 750 k: the 3 method," *Review of Scientific Instruments*, vol. 61, no. 2, pp. 802–808, 1990.

Cahill, D. G., Braun, P. V., Chen, G., Clarke, D. R., Fan, S., Goodson, K. E., Keblinski, P., King, W. P., Mahan, G. D., Majumdar, A., *et al.*, "Nanoscale thermal transport. ii. 2003–2012," *Applied Physics Reviews*, vol. 1, no. 1, p. 011305, 2014.

Cahill, D. G., Ford, W. K., Goodson, K. E., Mahan, G. D., Majumdar, A., Maris, H. J., Merlin, R., and Phillpot, S. R., "Nanoscale thermal transport," *Journal of Applied Physics*, vol. 93, no. 2, pp. 793–818, 2003.

Cahill, D. G. and Pohl, R. O., "Thermal conductivity of amorphous solids above the plateau," *Phys. Rev. B*, vol. 35, pp. 4067–4073, Mar 1987.

Cheney, B., "Introduction to scanning electron microscopy," *Materials Engineering department San Jose State University*, 2007.

Chopra, K. L., Bobb, L. C., and Francombe, M. H., "Electrical resistivity of thin singlecrystal gold films," *Journal of Applied Physics*, vol. 34, no. 6, pp. 1699–1702, 1963.

Costescu, R. M., Wall, M. A., and Cahill, D. G., "Thermal conductance of epitaxial interfaces," *Physical Review B - Condensed Matter and Materials Physics*, vol. 67, no. 5, pp. 1–5, 2003.

Dalton, P. D., Calvet, J. L., Mourran, A., Klee, D., and Möller, M., "Melt electrospinning of poly-(ethylene glycol-block-ϵ-caprolactone)," *Biotechnology Journal*, vol. 1, no. 9, pp. 998–1006, 2006.

Dalton, P. D., Grafahrend, D., Klinkhammer, K., Klee, D., and Möller, M., "Electrospinning of polymer melts: Phenomenological observations," *Polymer*, vol. 48, no. 23, pp. 6823–6833, 2007.

Dong, H., Nyame, V., MacDiarmid, A. G., and Jones Jr., W. E., "Polyaniline/poly(methyl methacrylate) coaxial fibers: The fabrication and effects of the solution properties on the morphology of electrospun core fibers," *Journal of Polymer Science Part B: Polymer Physics*, vol. 42, no. 21, pp. 3934–3942, 2004.

Eaton, P. and West, P., *Atomic force microscopy*. Oxford University Press, 2010.

Feser, J. P., Liu, J., and Cahill, D. G., "Pump-probe measurements of the thermal conductivity tensor for materials lacking in-plane symmetry," *Review of Scientific Instruments*, vol. 85, no. 10, 2014.

Fridrikh, S. V., Yu, J. H., Brenner, M. P., and Rutledge, G. C., "Controlling the Fiber Diameter during Electrospinning," *Physical Review Letters*, vol. 90, no. 14, p. 4, 2003.

Gaillard, C., Stadelmann, P. A., Plummer, C. J. G., and Fuchs, G., "Practical method for high-resolution imaging of polymers by low-voltage scanning electron microscopy," *Scanning*, vol. 26, no. 3, pp. 122–130, 2004.

Hu, X. J., Padilla, A. A., Xu, J., Fisher, T. S., and Goodson, K. E., "3-Omega Measurements of Vertically Oriented Carbon Nanotubes on Silicon," *Journal of Heat Transfer*, vol. 128, no. 11, p. 1109, 2006. [Online]. Available: http://heattransfer.asmedigitalcollection.asme.org/article.aspx?articleid=1448515

Huebner, A. L. and Chu, H. N., "Instability and breakup of charged liquid jets," *Journal of Fluid Mechanics*, vol. 49, no. 2, pp. 361–372, 1971.

Jagtap, R. and Ambre, A., "Overview literature on atomic force microscopy (afm): Basics and its important applications for polymer characterization," 2006.

Jiji, L. M., "Microscale conduction," *Heat Conduction: Third Edition*, vol. 35, pp. 347–401, 2009.

Ju, Y., Kurabayashi, K., and Goodson, K., "Thermal characterization of anisotropic thin dielectric films using harmonic joule heating," *Thin Solid Films*, vol. 339, no. 1, pp. 160 – 164, 1999.

Koh, Y. K. and Cahill, D. G., "Frequency dependence of the thermal conductivity of semiconductor alloys," *Physical Review B - Condensed Matter and Materials Physics*, vol. 76, no. 7, pp. 1–5, 2007.

Li, D. and Xia, Y., "Electrospinning of nanofibers: Reinventing the wheel?" *Advanced Materials*, vol. 16, no. 14, pp. 1151–1170, 2004.

Liu, W. L., Borca-Tasciuc, T., Chen, G., Liu, J. L., and Wang, K. L., "Anisotropic thermal conductivity of ge quantum-dot and symmetrically strained si/ge superlattices," *Journal of Nanoscience and Nanotechnology*, vol. 1, no. 1, pp. 39–42, 2001.

Lu, C., Wai, S., Du, H., Li, J., Gan, L., Zhang, X., Chu, X., Yao, Y., Li, B., and Kang, F., "Thermal conductivity of electrospinning chain-aligned polyethylene oxide (PEO)," *Polymer*, vol. 115, pp. 52–59, 2017.

Luu, Y. K., Kim, K., Hsiao, B. S., Chu, B., and Hadjiargyrou, M., "Development of a nanostructured DNA delivery scaffold via electrospinning of PLGA and PLA-PEG block copolymers," *Journal of Controlled Release*, vol. 89, no. 2, pp. 341–353, 2003.

Lyeo, H. K., Cahill, D. G., Lee, B. S., Abelson, J. R., Kwon, M. H., Kim, K. B., Bishop, S. G., and Cheong, B. K., "Thermal conductivity of phase-change material Ge 2 Sb 2 Te 5," *Applied Physics Letters*, vol. 89, no. 15, pp. 87–90, 2006.

Nayak, R., Kyratzis, I. L., Truong, Y. B., Padhye, R., Arnold, L., Peeters, G., Nichols, L., and O'Shea, M., "Fabrication and characterisation of nanofibres by meltblowing and melt electrospinning," *Advanced Materials*, vol. 472, pp. 1294–1299, 3 2012.

Putnam, S. A., Cahill, D. G., Ash, B. J., and Schadler, L. S., "High-precision thermal conductivity measurements as a probe of polymer/nanoparticle interfaces," *Journal of Applied Physics*, vol. 94, no. 10, pp. 6785–6788, 2003.

Putti, M., Simonet, M., Solberg, R., and Peters, G. W., "Electrospinning poly(ϵ-caprolactone) under controlled environmental conditions: Influence on fiber morphology and orientation," *Polymer (United Kingdom)*, vol. 63, pp. 189–195, 2015. [Online]. Available: http://dx.doi.org/10.1016/j.polymer.2015.03.006

Reneker, D. H. and Yarin, A. L., "Electrospinning jets and polymer nanofibers," *Polymers with aligned carbon nanotubes: Active composite materials*, vol. 49, no. 10, pp. 2387–2425, 2008.

Roduner, E., "Size matters: why nanomaterials are different," *Chem. Soc. Rev.*, vol. 35, pp. 583–592, 2006.

Schmidt, A. J., Chen, X., and Chen, G., "Pulse accumulation, radial heat conduction, and anisotropic thermal conductivity in pump-probe transient thermoreflectance," *Review of Scientific Instruments*, vol. 79, no. 11, 2008.

Slack, G. A. and Glassbrenner, C. J., "Thermal conductivity of Si and Ge from 3K to the melting point," *Physical Review*, vol. 1431, 1964. [Online]. Available: https://journals.aps.org/pr/pdf/10.1103/PhysRev.134.A1058

Taylor, G. I., "Disintegration of water drops in an electric field," *Proceedings of the Royal Society of London. Series A. Mathematical and Physical Sciences*, vol. 280, no. 1382, pp. 383–397, 1964.

Taylor, G. I. and Dyke, M. D. V., "Electrically driven jets," *Proceedings of the Royal Society of London. A. Mathematical and Physical Sciences*, vol. 313, no. 1515, pp. 453–475, 1969.

Thomas, V., Jose, M. V., Chowdhury, S., Sullivan, J. F., Dean, D. R., and Vohra, Y. K., "Mechano-morphological studies of aligned nanofibrous scaffolds of polycaprolactone fabricated by electrospinning," *Journal of Biomaterials Science, Polymer Edition*, vol. 17, no. 9, pp. 969–984, 2006.

Thompson, C., Chase, G., Yarin, A., and Reneker, D., "Effects of parameters on nanofiber diameter determined from electrospinning model," *Polymer*, vol. 48, no. 23, pp. 6913 – 6922, 2007. [Online]. Available: http://www.sciencedirect.com/science/article/pii/S0032386107009275

Tsai, P. P., Schreuder-Gibson, H., and Gibson, P., "Different electrostatic methods for making electret filters," *Journal of Electrostatics*, vol. 54, no. 3-4, pp. 333–341, 2002.

Verreck, G., Chun, I., Rosenblatt, J., Peeters, J., Van Dijck, A., Mensch, J., Noppe, M., and Brewster, M. E., "Incorporation of drugs in an amorphous state into electrospun nanofibers composed of a water-insoluble, nonbiodegradable polymer," *Journal of Controlled Release*, vol. 92, no. 3, pp. 349–360, 2003.

Wang, J. L., Gu, M., Zhang, X., and Song, Y., "Thermal conductivity measurement of an individual fibre using a T type probe method," *Journal of Physics D: Applied Physics*, vol. 42, no. 10, 2009.

Wilson, A., "Autofluorescent imaging and target ablation," U.S. Patent 8 160 680, Apr. 17, 2012.

Xu, C. Y., Inai, R., Kotaki, M., and Ramakrishna, S., "Aligned biodegradable nanofibrous structure: A potential scaffold for blood vessel engineering," *Biomaterials*, vol. 25, no. 5, pp. 877–886, 2004.

Yamane, T., Nagai, N., Katayama, S.-i., and Todoki, M., "Measurement of thermal conductivity of silicon dioxide thin films using a 3-omega method," *Journal of Applied Physics*, vol. 91, no. 12, pp. 9772–9776, 2002.

Yang, C., Yu, D.-G., Pan, D., Liu, X.-K., and Xia, "Electrospun ph-sensitive coreshell polymer nanocomposites fabricated using a tri-axial process," *Acta Biomaterialia*, vol. 35, pp. 77 – 86, 2016.

Yarin, A. L., Kataphinan, W., and Reneker, D. H., "Branching in electrospinning of nanofibers," *Journal of Applied Physics*, vol. 98, no. 6, 2005.

Yarin, A. L., Koombhongse, S., and Reneker, D. H., "Bending instability in electrospinning of nanofibers," *Journal of Applied Physics*, vol. 89, no. 5, pp. 3018–3026, 2001.

Zeng, J., Xu, X., Chen, X., Liang, Q., Bian, X., Yang, L., and Jing, X., "Biodegradable electrospun fibers for drug delivery," *Journal of Controlled Release*, vol. 92, no. 3, pp. 227–231, 2003.

Zhang, X., Fujiwara, S., and Fujii, M., "Measurements of thermal conductivity and electrical conductivity of a single carbon fiber," *International Journal of Thermophysics*, vol. 21, no. 4, pp. 965–980, 2000.